Plant Physiology Increases the Magnitude and Spread of the Transient Climate Response to CO_2 in CMIP6 Earth System Models

Claire Marie Zarakas

A thesis
submitted in partial fulfillment of the
requirements for the degree of

Master of Science

University of Washington
2020

Committee:

Abigail Swann

Kyle Armour

Gerard Roe

Program Authorized to Offer Degree:

Atmospheric Sciences

University of Washington

Abstract

Plant Physiology Increases the Magnitude and Spread of the Transient Climate Response to CO_2 in CMIP6 Earth System Models

Claire Marie Zarakas

Chair of the Supervisory Committee:
Abigail Swann
Department of Atmospheric Sciences

Increasing concentrations of CO_2 in the atmosphere not only influence climate through CO_2's effect as a greenhouse gas but also through its impact on plants. Plants respond to atmospheric CO_2 concentrations in several ways that can alter surface energy and water fluxes and thus surface climate, including changes in stomatal conductance, water use, and canopy leaf area. These plant physiological responses are already embedded in most Earth System models, and a robust literature demonstrates that they can affect global-scale temperature. However, the physiological contribution to transient warming has yet to be assessed systematically in Earth System models. Here this gap is addressed using carbon cycle simulations from the 5th and 6th phases of the Coupled Model Intercomparison Project (CMIP) to isolate the radiative and physiological contributions to the transient climate response (TCR). In CMIP6 models, the physiological effect contributes 0.12°C (σ: 0.09°C; range: 0.02 - 0.29°C) of warming to the TCR, corresponding to 6.1% of the full TCR (σ: 3.8%; range: 1.4 - 13.9%). Moreover, variation in the physiological contribution to the TCR across models contributes disproportionately more to the inter-model spread of TCR estimates than it does to the mean. The largest contribution of plant

physiology to CO_2-forced warming – and the inter-model spread in warming – occurs over land, especially in forested regions.

TABLE OF CONTENTS

LIST OF FIGURES

LIST OF TABLES

ACKNOWLEDGMENTS

I would like to thank my advisor, Abigail Swann, for her exceptional mentorship, advising, enthusiasm, and support. I would also like to thank my other collaborators on this project - Marysa Laguë, Kyle Armour, and James Randerson - for their thoughtful feedback and contributions to this research. I also appreciate the guidance from my thesis committee - Abigail Swann, Kyle Armour, and Gerard Roe – and thank them for helpful discussions and feedback related to this project. Funding support for this research came from the University of Washington Program on Climate Change Fellowship, the Department of Energy Computational Science Graduate Fellowship (DE-SC0020347), and the National Science Foundation AGS-1553715 to the University of Washington.

I am very grateful to the many people who have made the department of Atmospheric Sciences and Ecoclimate lab a welcoming community and engaging place to do research – a special thanks to the Ecoclimate lab members Greta Shum, Jennifer Hsiao, Marysa Laguë, Sam Pennypacker, Lucas Vargas Zeppetello, and Fiona Lo; my cohort Yuk Chun Chan, Tyler Cox, Andrew DeLaFrance, Carley Fredrickson, Lily Hahn, Daniel Lloveras, Jacqueline Nugent, Phil Rund, Clayton Sasaki, Greta Shum, Adam Sokol, Lindsey Taylor, Sami Turbeville, and Mingcheng Wang; and the Atmospheric Sciences staff.

Finally, I am thankful to my family, Doug, and friends in and beyond Seattle for their love and support.

Chapter 1.
INTRODUCTION

Increasing concentrations of atmospheric CO_2 alter global temperature through both CO_2's role as a greenhouse gas within the atmosphere (radiative effect) and through plants' response to CO_2 at the land surface (physiological effect). Plants respond to atmospheric CO_2 concentrations by regulating their stomata (pores on the leaves which modulate the exchange of CO_2 and water vapor between the leaf and the atmosphere), changing water use, adjusting canopy leaf area, and ultimately, changing species composition and vegetation cover. These plant physiological responses to higher CO_2 can physically influence land surface temperature by altering land evapotranspiration, surface albedo, and surface roughness, which are important controls over the fluxes of water and energy between the land surface and the atmosphere. Here we use the term "physiological effect" to encompass the net biogeophysical effect of all plant responses to increasing CO_2, but note that in some previous studies (e.g. Skinner et al. 2018) the term refers solely to the effect of changes in stomatal conductance. The physiological effect in this study may therefore be smaller than some previous estimates (e.g., Skinner et al. 2018; Cao et al. 2010) because increases in leaf area can counteract the influence of changes in stomatal conductance on land evapotranspiration.

Plant responses to CO_2 modulate land evapotranspiration through two opposing mechanisms. Higher concentrations of CO_2 in the atmosphere provide a larger gradient over which CO_2 diffuses into the interior airspace of leaves. As a result, most plant types close their stomata in response to increasing CO_2, thereby decreasing transpiration per unit of leaf area (Field et al. 1995). In contrast, photosynthetic rates under some environmental conditions are limited by access to CO_2, and in these instances more CO_2 can lead to higher rates of

photosynthesis, which is often referred to as CO_2 fertilization. CO_2 fertilization tends to either have no influence on canopy leaf area or to increase canopy leaf area (Norby and Zak 2011; Donohue et al. 2013), which increases transpiration. The physiological effect's net influence on land evapotranspiration therefore depends on the relative magnitude of the stomatal response and the leaf area response, as well as the extent to which vegetation influences land-atmosphere interactions in a given region (Lian et al. 2018). Most Earth System models (ESMs; Swann et al. 2016; Lemordant et al. 2018) and field experiments (Hungate et al. 2002; Leakey et al. 2009) suggest that the stomatal response term dominates in areas with moderate to high leaf area, leading to a net decrease in land evapotranspiration. However, future projections of photosynthetic rates, leaf growth rates, and thus transpiration remain highly uncertain (Friedlingstein et al. 2006; Anav et al. 2013; Piao et al. 2013; Smith et al. 2016; Lian et al. 2018).

Physiologically-driven reductions in evapotranspiration can warm local land temperatures directly by decreasing evaporative cooling, as well as indirectly through influences on low level humidity, cloud cover, and precipitation. Recent modeling studies have demonstrated that physiologically-driven decreases in land evapotranspiration can reduce cloud cover by decreasing low level relative humidity (Doutriaux-Boucher et al. 2009; Andrews et al. 2011, 2012; Arellano et al. 2012; Lemordant et al. 2018), which amplifies regional physiologically-driven warming. If the leaf area response were to dominate over stomatal responses, the resulting increase in evapotranspiration could decrease land temperatures through these same mechanisms. Physiologically-forced drying of the boundary layer and warming of the land surface can not only modulate local surface energy fluxes, but can also impact large scale atmospheric dynamics and regional precipitation (Kooperman et al. 2018a; Langenbrunner et al. 2019; Saint-Lu et al. 2019; Park et al. 2020).

In addition to influencing land surface temperature by altering evapotranspiration, the plant physiological response to CO_2 can also influence land surface temperature by altering land surface albedo. CO_2 fertilization generally decreases albedo (thereby increasing temperature) by increasing leaf area and, within dynamic vegetation models, by shifting plant functional types from grasses to trees (Bala et al. 2006; Andrews et al. 2019). Expansion of forests in boreal and Arctic regions can result in especially large albedo decreases (Betts 2000; Bala et al. 2006; O'ishi et al. 2009; Andrews et al. 2019; Xu et al. 2020) because increases in foliage mask bright snow.

The global-scale temperature implications of plants' physiological responses to CO_2 have been long acknowledged. Sellers et al. (1996) were the first to quantify physiologically-driven warming by coupling a biosphere model to an atmosphere model, finding that under a doubling of CO_2 the physiological effect increased global land temperature by about 0.3°C and mean global temperature by about 0.1°C. Since then, multiple modeling studies have demonstrated that the plant physiological response tends to increase land temperature in most modern ESMs on annual timescales (Betts et al. 2007; Cao et al. 2010; Andrews et al. 2011; Arora et al. 2013; Swann et al. 2016; Lemordant et al. 2016, 2018; Arora et al. 2019) and during heatwaves (Lemordant et al. 2016; Skinner et al. 2018; Lemordant and Gentine 2019). In particular, as part of their analysis to disentangle carbon-concentration and carbon-climate feedbacks, Arora et al. (2013, 2019) show that the physiological effect drives modest transient global warming in most CMIP5 (Arora et al. 2013; Figure 2a-c) and CMIP6 (Arora et al. 2019; Figure 4a-c) ESMs, although they explicitly quantify the physiological warming only for the multi-model mean.

Despite this demonstrated physiological influence on global surface temperatures, the physiological effect has received limited recognition in the climate dynamics literature. Although

plants' physiological responses to CO_2 are already embedded in many ESMs which are used to estimate the transient climate response (TCR) and equilibrium climate sensitivity (ECS), studies that explicitly quantify the physiological contribution to such global-scale climate sensitivity metrics have been limited to ESMs from a few individual modeling centers (summarized in Table A1; Sellers et al. 1996; Betts et al. 1997; Cox et al. 1999; Douville et al. 2000; Levis et al. 2000; Bala et al. 2006; Betts et al. 2007; Doutriaux-Boucher et al. 2009; Boucher et al. 2009; Cao et al. 2009; O'ishi et al. 2009; Cao et al. 2010; Andrews et al. 2011; Pu and Dickinson 2012). Physiology's contribution to the TCR has not been systematically assessed across models and Coupled Model Intercomparison Project (CMIP) phases.

Additionally, past studies in the climate sensitivity literature have not specifically quantified the physiological contribution to the TCR using the same experimental methodology from which the full TCR is calculated. For example, baseline levels of CO_2 have ranged from 280 to 400 ppm across experiments (Table A1) and the physiological effect's influence on temperature has been analyzed from both abrupt (Doutriaux-Boucher et al. 2009; Cao et al. 2010; Andrews et al. 2011) and transient (Bala et al. 2006; Boucher et al. 2009) CO_2 perturbations. Modeling studies have also differed in whether they include both the stomatal and leaf area components of the physiological effect or only the stomatal component. While these different experimental designs have provided insights into the mechanisms and timescales of the physiological effect's influence on climate, they do not provide systematic estimates of the full physiological contribution to the TCR across ESMs.

The lack of systematic inter-model comparison of the physiological contribution to the TCR is a problematic gap in the existing literature because past work suggests that physiologically-driven warming differs across models. Arora et al. (2013, 2019) documented that

the magnitude of global physiologically-driven warming varies across models, reflecting that models differ both in how plants respond to increasing CO_2 (Friedlingstein et al. 2006; Anav et al. 2013; Piao et al. 2013; Smith et al. 2016; Lian et al. 2018) and in how the atmosphere responds to perturbations to the land surface energy budget (Andrews et al. 2009; Devaraju et al. 2018). This suggests that inter-model disagreement about the magnitude of physiologically-driven warming may be an unrecognized contributor to inter-model spread in CO_2-forced warming. Additionally, poor model agreement on the magnitude of physiologically-driven warming would mean that an estimate derived from a single model may not capture the true multi-model mean. To address this gap, we use standardized carbon cycle model simulations from the CMIP phase 5 and 6 archives to assess (1) the magnitude of the physiological effect's influence on temperature across models, (2) whether trends in the physiological effect contribute to the increase in the TCR noted for many recent models (Andrews et al. 2019; Gettelman et al. 2019; Golaz et al. 2019; Flynn and Mauritsen 2020), (3) the spatial pattern of physiologically-driven temperature changes, (4) how physiological processes contribute to variability in multi-model estimates of the TCR, and (5) the mechanisms through which the physiological effect influences temperature.

Chapter 2.
METHODS

2.1. CMIP Experiments

As part of CMIP5 and CMIP6, modeling groups performed three concentration-driven experiments (summarized in Table 1) in which CO_2 concentrations increase by 1 percent per year from pre-industrial levels (284.3 ppm) to a quadrupling of CO_2 (1144.9 ppm), while all other forcings remain at pre-industrial levels. The spatial pattern of vegetation in these simulations comes from the pre-industrial era; this spatial pattern remains constant throughout the simulation except for in land models with dynamic vegetation (Tables B1 and B2), where the distribution of plant functional types changes based on climate and resource availability. In one set of simulations, referred to here as 'FULL' (CMIP6 experiment '1pctCO2'), both the atmosphere and carbon cycle (on land and in the oceans) experience increasing CO_2 concentrations. Additional experiments conducted as part of the Coupled Climate–Carbon Cycle Model Intercomparison Project (C4MIP; Friedlingstein et al. 2006; Jones et al. 2016) enable us to isolate how much the physiological and radiative effects of CO_2 each contribute to surface warming. In a set of C4MIP simulations, referred to here as 'RAD' (CMIP6 experiment '1pctCO2-rad'), only the atmosphere experiences increasing CO_2 concentrations, while the terrestrial and oceanic carbon cycles experience constant pre-industrial CO_2 concentrations. In another set of C4MIP simulations, referred to here as 'PHYS' (CMIP6 experiment '1pctCO2-bgc'), the radiative transfer submodels in the atmosphere experience constant pre-industrial CO_2 concentrations, while the land surface and ocean carbon cycle submodels experience the increasing CO_2 concentrations. We use the concentration-driven pre-industrial control

experiment (referred to here as 'PI', CMIP6 experiment 'piControl') as the baseline from which anomalies are calculated.

Experiment	CMIP5 Experiment Name	CMIP6 Experiment Name	Influence of CO_2 Concentration on:		
			Land	Ocean	Atmosphere
FULL	1pctCO2	1pctCO2	1% per year	1% per year	1% per year
PHYS	esmFixClim1	1pctCO2-bgc	1% per year	1% per year	Pre-industrial
RAD	exmFdbk1	1pctCO2-rad	Pre-industrial	Pre-industrial	1% per year
PI	piControl	piControl	Pre-industrial	Pre-industrial	Pre-industrial

Table 1. Summary of CMIP experiments used

2.2. Models

We analyze output from all ESMs that had uploaded near-surface air temperature monthly data for the FULL, PI, and PHYS and/or RAD experiment to the Earth System Grid by May 13, 2020. This consisted of 8 CMIP5 models (Table B1) and 12 CMIP6 models (Table B2). These models all include interactive representations of the carbon cycle; plants in these models respond to increasing CO_2 by changing leaf area, stomatal conductance, and, in some models, the location and distribution of plant functional types (indicated in Tables B1 and B2). Three models from CMIP6 have dynamic vegetation; however, we do not believe this is a large enough set of models to draw general conclusions about the impact of dynamic vegetation. In addition, one of these three models is UKESM1-0-LL which has a significantly larger physiologically-driven temperature response relative to other models, but it is unclear if this stronger temperature response is driven by dynamic vegetation.

Ocean responses to increasing CO_2 include changes in inorganic and biological carbon cycling, which have negligible direct influences on modeled ocean surface temperature. The only potential direct influences of ocean carbon cycle responses on ocean surface temperatures in the PHYS experiments are through changes in plankton community structure which can alter (1)

ocean biogeophysical properties and (2) the emission of gases and particles which influence aerosol formation (Hense et al. 2017). These effects are not represented in most models. We calculate multi-model mean maps after re-gridding model output to a consistent 0.9424° latitude by 1.25° longitude grid.

2.3. Calculation of Climate Sensitivity Metrics TCR and T140

We calculate the TCR as the change in globally averaged near-surface air temperature during the 20-year window centered on the time of CO_2 doubling (years 61-80 of the simulation where CO_2 concentration increases by 1% per year) relative to pre-industrial CO_2 concentrations. When using the PI experiment as a control, we account for model drift by subtracting the linear trend of PI years 1-140 following Gregory and Forster (2008), where year 1 corresponds to the year at which FULL, RAD, and PHYS were branched from PI. We refer to the physiological and radiative contributions to the full TCR as TCR_{PHYS} and TCR_{RAD}, respectively.

We also quantify the physiological and radiative contributions to the T140 metric (Gregory et al. 2015; Grose et al. 2018). We calculate T140 as the change in globally averaged near-surface air temperature during the 20-year window that ends at the time of CO_2 quadrupling (years 121-140 of the simulation where CO_2 concentration increases by 1% per year) relative to the linearly detrended PI experiment following Gregory et al. (2015).

We assess whether our estimates of physiologically-driven warming are robust relative to variability in the Earth System by comparing TCR_{PHYS} and $T140_{PHYS}$ to the distribution of 20-year running mean global temperatures in the full PI control experiments (Figure F1). In two of the CMIP6 models evaluated here (BCC-CSM2-MR and CNRM-ESM2-1), large, multidecadal (greater than 20 year) oscillations exist in the PI control (Figure F1; noted in Parsons et al. 2020). The magnitude of these oscillations greatly exceeds the magnitude of the TCR_{PHYS} signal, and

thus we cannot confidently quantify the TCR_{PHYS} for these two models. These models' large multidecadal PI oscillations also have implications for TCR_{FULL}, as they suggest that model TCR_{FULL} estimates may be strongly influenced by variability rather than only representing the CO_2-forced warming signal, since for these models smoothing out variability would require an averaging period of greater than 20 years.

2.4. Isolating Physiology's Influence on Temperature

We quantify the influence of the physiological effect in two ways: as the difference between the FULL and RAD simulations (FULL-RAD) and as the difference between the PHYS and PI simulations (PHYS-PI). Both represent physiology's influence on the TCR, but FULL-RAD includes any nonlinear interactions between the radiative and physiological effects of increasing CO_2, while PHYS-PI does not. For example, FULL-RAD would include the interaction between CO_2 fertilization and changes in leaf area (quantified as the leaf area index, LAI) induced by radiatively-driven warming. Warming generally increases vegetation productivity in high-latitudes that are temperature-limited under current conditions (Qian et al. 2010), thereby increasing leaf area (Keenan and Riley 2018), while some ESMs suggest warming may decrease vegetation productivity and leaf area in the tropics (Mahowald et al. 2016) where current temperatures are already near plants' optimal temperatures for photosynthesis. We focus on the FULL-RAD methodology in the main text because it emphasizes how much the physiological effect changes climate relative to what models would otherwise show from radiative forcing alone. Because FULL and RAD branch from the same point of the PI simulation, using FULL-RAD to quantify the physiological effect also avoids issues related to drift in the PI control. We discuss the nonlinearity between the radiative and physiological effects of CO_2 in more detail in Appendix C.

2.5. Partitioning Physiological Influences on Evapotranspiration

In order to partition the total physiologically-driven change in land evapotranspiration into its component physiological drivers, we derived Equation 1 (see Appendix D). The four terms on the right-hand side of Equation 1 indicate the land evapotranspiration change due to (1) changes in leaf area, (2) changes in stomatal conductance (approximated as changes in transpiration per leaf area), (3) interactions between changes in stomatal conductance and changes in leaf area, and (4) changes in land evaporation.

$$\Delta ET = \left(\frac{T}{L}\right)_{REF} (\Delta L) + L_{REF} \left(\Delta \frac{T}{L}\right) + \left(\Delta \frac{T}{L}\right)(\Delta L) + \Delta E \qquad \text{Equation 1}$$

where ET = evapotranspiration (mm/day); T = transpiration (mm/day); L = leaf area index (unitless); and E = evaporation (mm/day). The REF subscript indicates the value from the reference experiment without physiological responses to CO_2 (RAD for the FULL-RAD method and PI for the PHYS-PI method), and Δ indicates the physiologically-driven change (e.g. as calculated from FULL-RAD).

Chapter 3.
RESULTS

3.1. Physiology's Contribution to the TCR and T140

The radiative effect of CO_2 is, unsurprisingly, the dominant contributor to both the TCR and T140. However, we also find that the physiological response to increased CO_2 makes a non-negligible secondary contribution to the TCR and T140 in many CMIP5 and CMIP6 models (Figures 1 and 2). In CMIP6 models, the physiological effect contributes about 0.12°C (σ: 0.09°C; range: 0.02 - 0.29°C) to the TCR, corresponding to 6.1% of the full TCR (σ: 3.8%; range: 1.4 - 13.9%) (Table 2). For a few CMIP6 models (especially UKESM1-0-LL and CESM2), the physiological contribution to warming is quite large, accounting for over 10% of the total TCR (Table 2). Physiology-driven warming increases with increasing CO_2 concentration (Figure 1c), on average contributing 0.21°C (σ: 0.12°C; range: 0.03 - 0.45°C) to the T140 metric. On a percentage basis, the physiological effect contributes proportionally less to the T140 metric (4.9%; σ: 2.5%) than to the TCR, though this varies across models.

In CMIP5 models, the physiological effect contributes 0.14°C (σ: 0.16°C; range: 0.00 - 0.51°C) to the TCR, corresponding to 6.6% of the full TCR (σ: 6.3%; range: 0.1 - 20.1%). When comparing the same subset of eight models for which we have model output from both CMIP phases, physiologically-driven warming is comparable in CMIP5 and CMIP6 (Table 2). This suggests that the increases in TCR_{FULL} from CMIP5 to CMIP6 noted for many recent models (Andrews et al. 2019; Gettelman et al. 2019; Golaz et al. 2019; Flynn and Mauritsen 2020) were driven primarily by increases in TCR_{RAD} rather than TCR_{PHYS}. Physiology's relative contribution to the TCR decreased in most models (Table 2), due to many CMIP6 models' increased values of TCR_{RAD}.

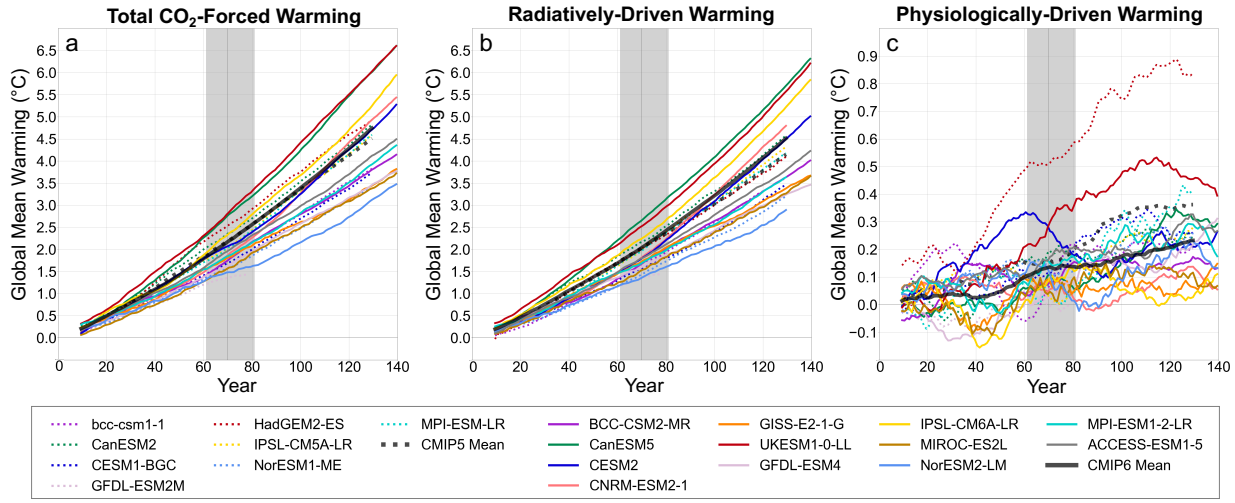

Figure 1. Time series of global mean temperature change for (a) all CO_2-forced warming, as calculated from FULL-PI, (b) the radiative contribution to global mean CO_2-forced warming, as calculated from RAD-PI, and (c) the physiological contribution to global mean CO_2-forced warming, as calculated from FULL-RAD. Time series in (a), (b), and (c) are smoothed with a 20-year rolling average. The dark gray vertical line marks the time of CO_2 doubling, and the light gray bar indicates the 20-year period surrounding the time of CO_2 doubling. Colors indicate modeling center and line types indicate CMIP phase (CMIP5: dashed; CMIP6: solid). Temperature changes for GFDL-ESM2M are only shown for years 1-70 because this model stopped ramping up CO_2 concentration after reaching 2xCO_2. Note that the set of models included in the average differs between CMIP5 and CMIP6, and that the y-axis scale in (c) differs from (a) and (b).

The multi-model mean TCR_{PHYS} values reported here are within the range of estimates from other studies (summarized in Table A1), but on the low side of this range likely for two reasons. First, many previous studies isolated the effect of the stomatal response on near-surface temperatures rather than the net effect of both the stomatal and leaf area responses (Table A1); we expect a larger temperature increase from the stomatal response alone than from the combined stomatal and leaf area responses because increases in leaf area counteract the stomatal response's influence on evapotranspiration. Second, our study is the first to compare TCR_{PHYS} across models (12 from CMIP6 and 8 from CMIP5), and the fact that the existing literature did not capture the full spread in TCR_{PHYS} across models underscores the importance of a multi-model approach.

The global mean TCR_{PHYS} signal is small in comparison to TCR_{FULL}, and it is statistically significant relative to the pre-industrial control for only 7 of 12 CMIP6 and 5 of 8 CMIP5 models at $2xCO_2$ (Table F1). By $4xCO_2$, the physiologically-driven warming signal emerges from the noise for more models (Figure F1), becoming statistically significant for 9 CMIP6 and 7 CMIP5 models (Table F1). The three CMIP6 models that are not statistically significant by $4xCO_2$ (CNRM-ESM2-1, BCC- CSM2-MR, and IPSL-CM6A-LR) are the three models with the most variability in the PI control of all the CMIP5 and CMIP6 models we analyze (Figure F1).

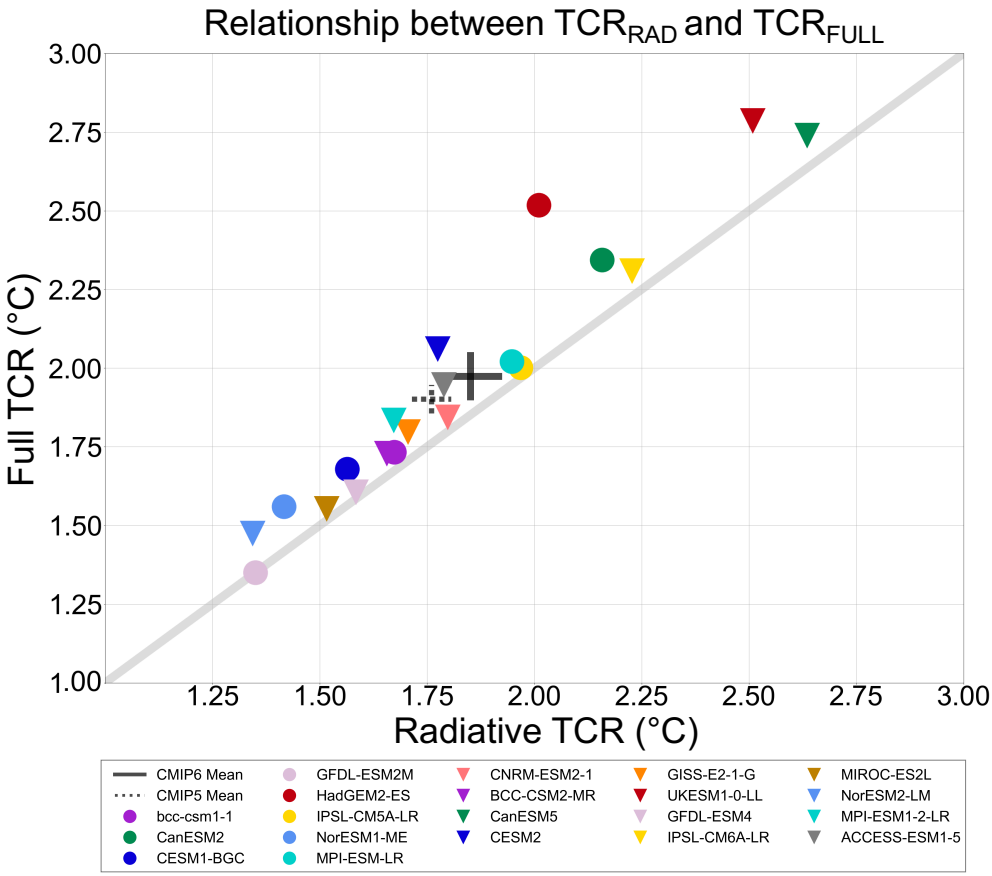

Figure 2. Relationship between TCR_{RAD} (RAD-PI) and TCR_{FULL} (FULL-PI). The gray 1:1 line is where we would expect all models to be if the TCR were entirely caused by the radiative effects of CO_2. The added warming from the physiological effect is the vertical distance between the gray 1:1 line and each point. Marker types indicate CMIP phase (CMIP5: circles; CMIP6: triangles) and colors indicate modeling center. Crosses demarcate the CMIP6 (solid) and CMIP5 (dashed) multi-model means, and the width of each cross corresponds to two times the ensemble mean standard deviation in global mean near-surface temperature from the preindustrial control.

Modeling Center	CMIP5 Model TCR								CMIP6 Model TCR							
	Model Name	FULL	RAD		PHYS-PI		FULL-RAD		Model Name	FULL	RAD		PHYS-PI		FULL-RAD	
		°C	°C	%	°C	%	°C	%		°C	°C	%	°C	%	°C	%
Beijing Climate Center (BCC)	bcc-csm1-1	1.73	1.67	96.5%	0.05	2.8%	0.06	3.5%	BCC-CSM2-MR	1.73	1.66	95.8%	0.54	31.4%	0.07	4.2%
Canadian Centre for Climate Modelling and Analysis (CCCma)	CanESM2	2.34	2.16	92.1%	0.15	6.5%	0.19	7.9%	CanESM5	2.74	2.64	96.2%	0.04	1.5%	0.10	3.8%
National Center for Atmospheric Research (NCAR)	CESM1-BGC	1.68	1.56	93.2%	0.11	6.6%	0.11	6.8%	CESM2	2.06	1.78	86.1%	0.11	5.2%	0.29	13.9%
NOAA Geophysical Fluid Dynamics Laboratory (NOAA-GFDL)	GFDL-ESM2M	1.35	1.35	99.9%	0.05	3.4%	0.00	0.1%	GFDL-ESM4	1.61	1.58	98.6%	0.17	10.7%	0.02	1.4%
Met Office Hadley Centre (MOHC)	HadGEM2-ES	2.52	2.01	79.9%	0.37	14.6%	0.51	20.1%	UKESM1-0-LL	2.79	2.51	90.0%	0.17	6.0%	0.28	10.0%
Institut Pierre Simon Laplace (IPSL)	IPSL-CM5A-LR	2.00	1.97	98.3%	0.11	5.6%	0.03	1.7%	IPSL-CM6A-LR	2.31	2.23	96.4%	0.17	7.3%	0.08	3.6%
Norwegian Climate Centre (NCC)	NorESM1-ME	1.56	1.42	90.8%	0.08	5.3%	0.14	9.2%	NorESM2-LM	1.48	1.34	91.0%	-	-	0.13	9.0%
Max Planck Institute for Meteorology (MPI-M)	MPI-ESM-LR	2.02	1.95	96.4%	0.20	9.9%	0.07	3.6%	MPI-ESM1-2-LR	1.84	1.67	91.1%	0.13	7.2%	0.16	8.9%
Commonwealth Scientific and Industrial Research Organisation (CSIRO)	-	-	-	-	-	-	-	-	ACCESS-ESM1-5	1.95	1.79	91.9%	0.21	10.7%	0.16	8.1%
Centre National de Recherches Météorologiques (CNRM-CERFACS)	-	-	-	-	-	-	-	-	CNRM-ESM2-1	1.84	1.80	97.5%	-0.15	-8.0%	0.05	2.5%
NASA Goddard Institute for Space Studies (NASA-GISS)	-	-	-	-	-	-	-	-	GISS-E2-1-G	1.80	1.71	94.9%	0.08	4.3%	0.09	5.1%
Japan Agency for Marine-Earth Science and Technology (JAMSTEC)	-	-	-	-	-	-	-	-	MIROC-ES2L	1.55	1.52	97.6%	0.07	4.8%	0.04	2.4%
Mean	**All Models**	**1.90**	**1.76**	**93.4%**	**0.14**	**6.8%**	**0.14**	**6.6%**	**All Models**	**1.97**	**1.85**	**93.9%**	**0.14**	**7.4%**	**0.12**	**6.1%**
	Consistent Model Subset	*1.90*	*1.76*	*93.4%*	*0.14*	*6.8%*	*0.14*	*6.6%*	*Consistent Model Subset*	*2.07*	*1.93*	*93.2%*	*0.19*	*9.9%*	*0.14*	*6.8%*
Standard Deviation	**All Models**	**0.40**	**0.30**	**6.3%**	**0.11**	**3.8%**	**0.16**	**6.3%**	**All Models**	**0.43**	**0.40**	**3.8%**	**0.16**	**9.5%**	**0.09**	**3.8%**
	Consistent Model Subset	*0.40*	*0.30*	*6.3%*	*0.11*	*3.8%*	*0.16*	*6.3%*	*Consistent Model Subset*	*0.50*	*0.47*	*4.2%*	*0.16*	*9.9%*	*0.10*	*4.2%*

Table 2. TCR_{FULL}, TCR_{RAD}, and TCR_{PHYS} by model, where TCR_{PHYS} is calculated by both PHYS-PI and FULL-RAD. The consistent model subset refers to the eight models for which the necessary model output is available for both CMIP5 and CMIP6. For the summary statistics in the last four rows, the percentages refer to the mean and standard deviations of the percent contributions across models.

3.2. Spatial Pattern of Physiologically-Driven Warming

The physiological effect only directly influences land surface properties, and thus the largest warming driven by the physiological effect occurs over land. In CMIP6 models, the physiological effect results in a land mean warming of 0.22°C at $2xCO_2$ and 0.41°C at $4xCO_2$, relative to a corresponding mean ocean warming of 0.09°C and 0.14°C respectively (Figure 3a). Physiologically-driven warming over land is also statistically significant for more ESMs than it is for the global mean at both $2xCO_2$ and $4xCO_2$ (Table F1). The spatial pattern of physiologically-driven warming that we find is consistent with other studies, which also show the greatest warming over land and modest ocean warming (Table A1).

The greatest mean physiologically-driven warming occurs over boreal forests and non-glaciated high-latitude land, followed by temperate and tropical forested regions. The agreement across models is reasonably high - at least 8 of 12 CMIP6 models agree that the physiological effect results in warming in these three biomes at $2xCO_2$ (Figure E1) and 10 of 12 CMIP6 models show warming in these biomes at $4xCO_2$ (Figure E2). Relative to radiatively-driven warming, physiology also contributes more to land warming than ocean warming, with physiological forcing constituting a mean 7.4% of total CO_2-forced land warming at $2xCO_2$ compared to 4.5% of ocean warming (Figure 3b). The physiological effect therefore amplifies the land/ocean warming contrast: at $2xCO_2$ non-glaciated land warms faster than the ocean with a mean ratio of 1.60 for the RAD simulations from CMIP6, whereas the mean land/ocean warming contrast for the FULL simulations is 1.64, due to the addition of the physiological effect (Figure 4). This physiologically-driven enhancement of the land/ocean warming contrast was previously demonstrated for Met Office Hadley Centre models (Joshi et al. 2008; Dong et al. 2009), and we

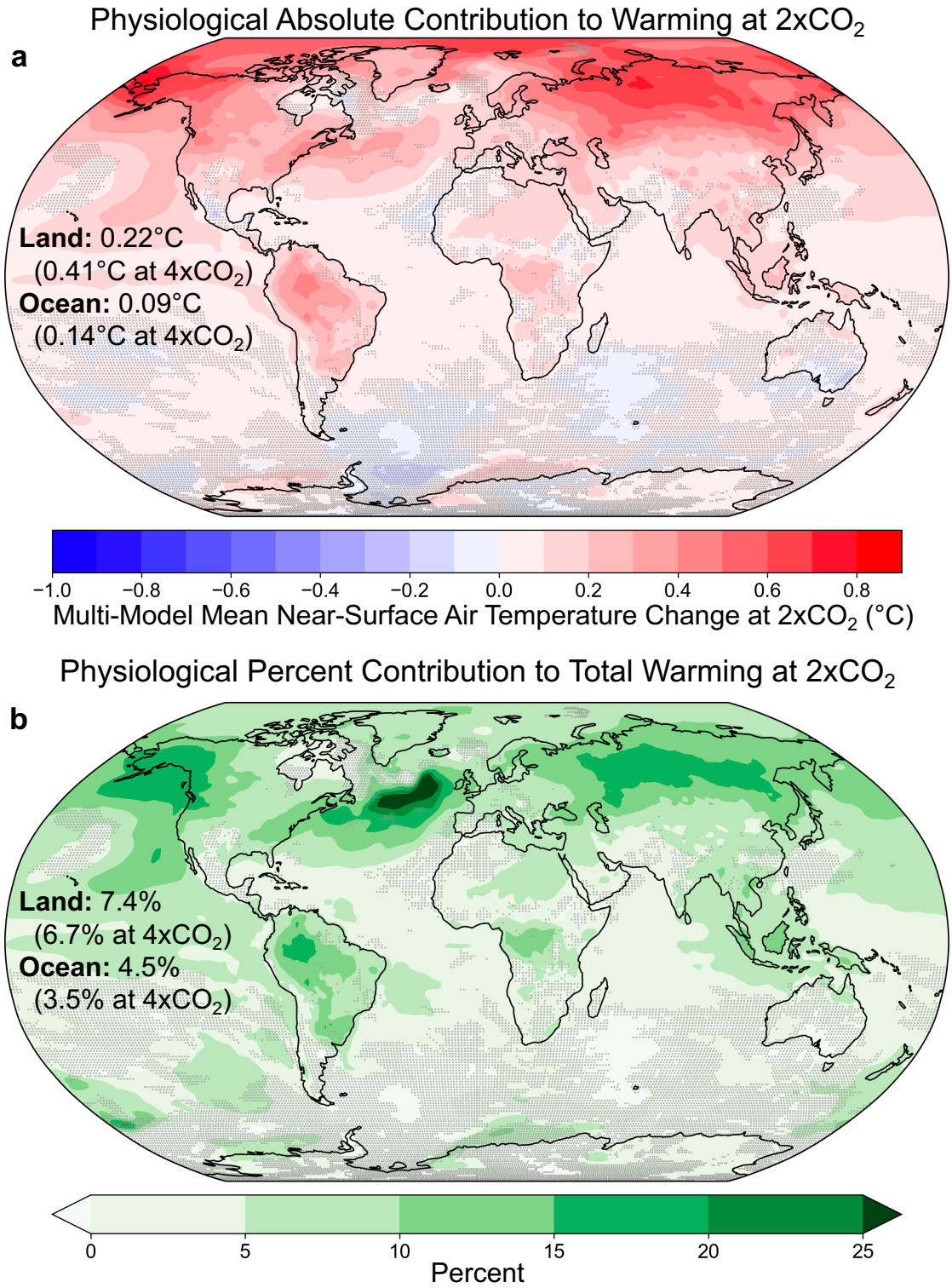

Figure 3. Spatial pattern of (a) absolute physiologically-driven warming and (b) physiological percent contribution to total warming at 2xCO_2, where physiologically-driven warming is calculated by FULL-RAD. Multi-model means include the 12 CMIP6 models. Stippling indicates regions where less than 8 out of the 12 models agree on the sign of change.

show here that this warming contrast is robust across most CMIP models. In two models the physiological effect reduces the land/ocean warming contrast (Figure 4). These outliers may result from large leaf area increases counteracting the influence of stomatal closure on evapotranspiration (resulting in minimal net physiologically-driven change in evapotranspiration or even small increases in evapotranspiration) or from large multi-decadal variability in some models (Figure F1) overwhelming the physiological signal.

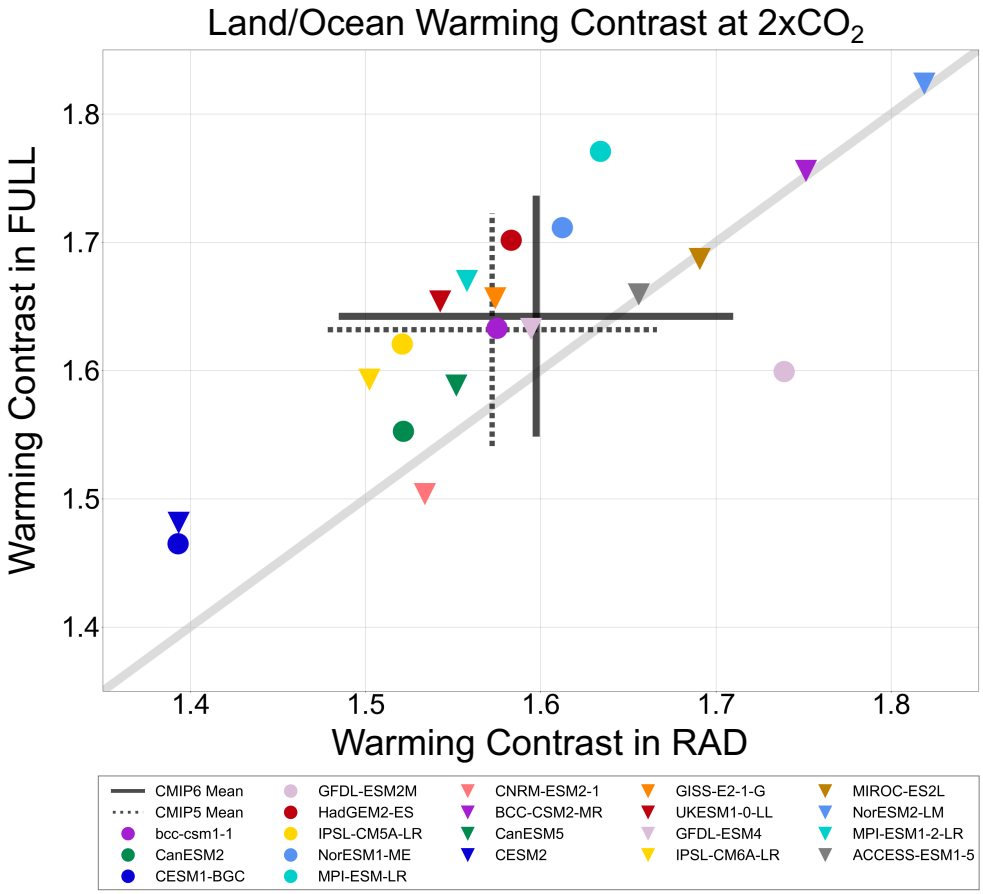

Figure 4. The relationship between the land/ocean warming contrast (the ratio of the change in mean non-glaciated land near-surface air temperature to the change in mean ocean near-surface air temperature) from RAD (RAD-PI) and FULL (FULL-PI) at 2xCO_2. The gray 1:1 line is where we would expect all models to be if the warming contrast were entirely caused by the radiative effects of CO_2. Physiology's addition to the warming contrast is the vertical distance between the gray 1:1 line and each point. Marker types indicate CMIP phase (CMIP5: circles; CMIP6: triangles) and colors indicate modeling center as in Figure 2. Crosses demarcate multi-model means, where the width of each cross is two standard deviations across models. Note that the set of models included in the average differs between CMIP5 and CMIP6.

The larger absolute and relative physiologically-driven warming over non-glaciated land is consistent with the physiological effect directly influencing land surface properties in regions with plant cover, while influencing glaciated land and oceans only indirectly through changes in heat transport, clouds, and other aspects of climate dynamics. Though the remote influence of physiological forcing on oceans and glaciated land is relatively modest, most models agree that the physiological effect results in mean warming of near-surface oceanic air and ocean surface layers. The regions of the most robust physiologically-driven oceanic warming across models are the western North Atlantic, equatorial Pacific, equatorial Indian Ocean, and high latitude Pacific.

Byrne and O'Gorman (2018) suggest that increases in the near surface land-ocean temperature contrast are causally driven by temperature change over the ocean. However, the physiologically-driven enhanced land-ocean contrast, where the only initial difference is over the land surface, shows that land surface processes can also initiate the feedback loop of decreasing relative humidity over land leading to a larger increase in temperature over land relative to over ocean. The potential to initiate this loop through land processes is noted by Byrne and O'Gorman (2016), and we further emphasize that point here. It is important to acknowledge the physiological effect's greater relative contribution to land warming because land warming (rather than global mean warming) is the most relevant metric for many societal climate impacts.

3.3. Physiology's Contribution to Uncertainty in CO_2-Forced Warming

The magnitude of global physiologically-driven warming varies significantly across models (Figures 1, 2, and E3) and this uncertainty contributes to the inter-model spread of TCR estimates. In the CMIP6 models analyzed here, the radiative effect alone explains about 91.9% of the standard deviation in the TCR across models (Table 3), with the physiological effect contributing the remaining 8.1%. Thus, the impact of the physiological effect on model-to-model

variability is disproportionately large relative to its contribution to the mean (8.1% for the standard deviation versus 6.1% for the mean). The physiological effect accounts for relatively less inter-model spread in the T140 metric (Table 3), consistent with other work (Geoffroy et al. 2012, Lutsko and Popp 2019) demonstrating that radiative feedbacks contribute increasingly more to inter-model disagreement in warming with increasing time in the transient 1pctCO_2 experiment.

CMIP Phase	Region	2xCO_2 (TCR)		4xCO_2 (T140)	
		FULL-PI	RAD-PI	FULL-PI	RAD-PI
CMIP6	Global	0.43°C	0.40°C (92%)	1.02°C	0.98°C (96%)
	Land[1]	0.58°C	0.50°C (86%)	1.32°C	1.19°C (90%)
	Ocean	0.38°C	0.36°C (95%)	0.91°C	0.90°C (99%)
CMIP5	Global	0.40°C	0.30°C (76%)	1.09°C	0.95°C (87%)
	Land[1]	0.58°C	0.39°C (68%)	1.55°C	1.24°C (80%)
	Ocean	0.33°C	0.27°C (81%)	0.91°C	0.84°C (91%)

Table 3. Drivers of inter-model spread in global mean warming, as quantified by the standard deviation.

The physiological effect contributes more to uncertainty in CO_2-forced warming over land. Averaged across all non-glaciated land, the physiological effect explains about 13.6% of the standard deviation in mean land warming across models at 2xCO_2 in CMIP6 (Table 3). In some highly forested land regions (tropical Africa, northwestern South America, and the southeastern United States), inter-model disagreement in local warming at 2xCO_2 is driven by approximately equal contributions of uncertainty from physiologically- and radiatively-forced warming (Figure 5). These results suggest that the physiological effect is a non-negligible contributor to inter-model spread in the TCR and regional land CO_2-forced warming at 2xCO_2.

[1] Non-glaciated land

However, some of these pre-industrial forested regions are largely deforested in the present day, which means that in scenario-based future projections the physiological effect may contribute less to uncertainty in these regions than Figure 5 implies.

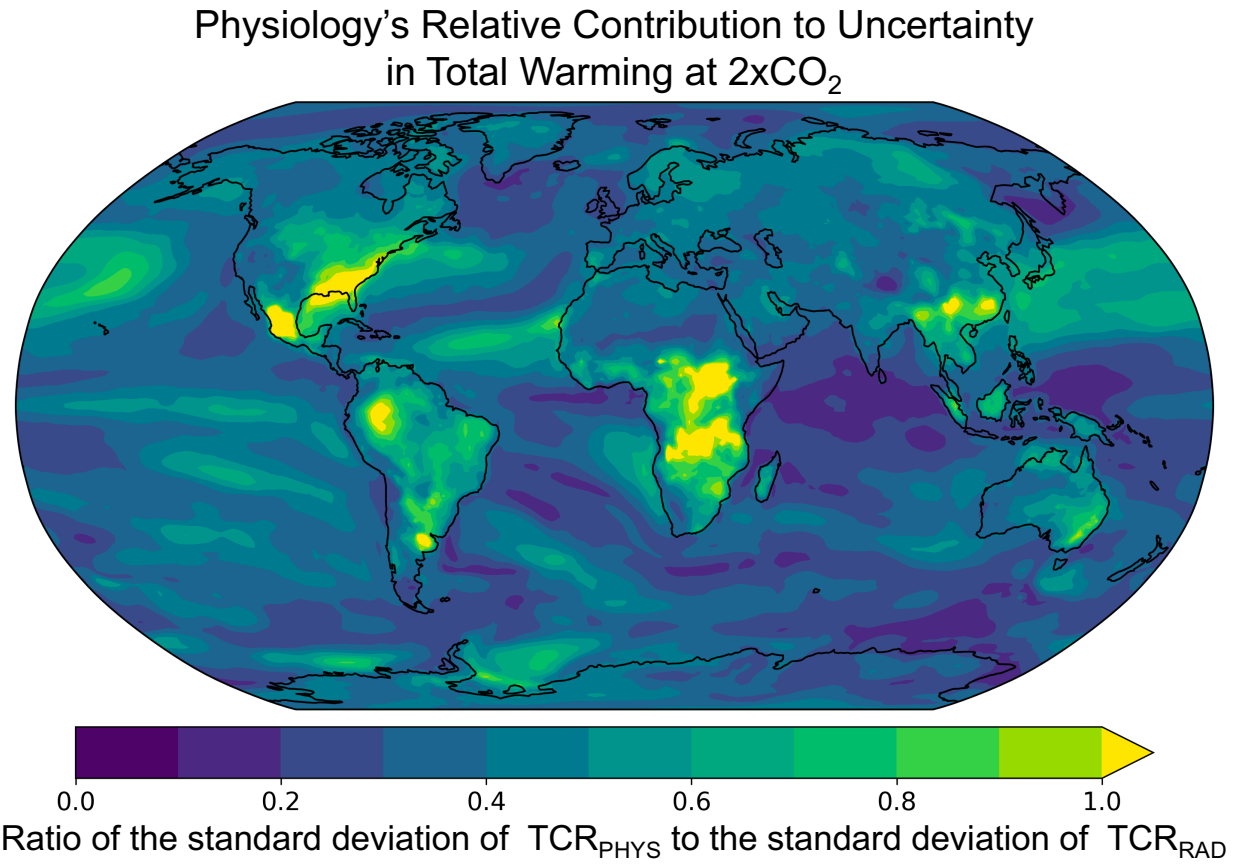

Figure 5. Spatial pattern of physiology's relative contribution to inter-model spread in CO_2-forced warming, as quantified by the ratio of the standard deviation (σ; at each grid cell, across models) of physiologically-forced warming (calculated from FULL-RAD) to σ of radiatively-forced warming (calculated from RAD-PI) at 2xCO_2 for CMIP6 models, i.e. $\sigma_{PHYS}(lat, lon)/\ \sigma_{RAD}(lat, lon)$. A value of 1 means that the physiological and radiative effects of CO_2 contribute equally to the total uncertainty in local warming at 2xCO_2 across models

The physiological effect contributes less to uncertainty in CO_2-forced warming over the ocean, explaining about 5% of the standard deviation of the mean ocean warming across models at 2xCO_2 in CMIP6 (Table 3). In all oceanic regions, inter-model disagreement in CO_2-forced warming is driven more by radiative processes than the physiological effect (Figure 5). However, Figure 5 suggests that physiology is a significant secondary driver of inter-model disagreement

in the magnitude of CO_2-forced warming in some ocean regions (e.g. North Atlantic and North Pacific), possibly due to inter-model disagreement in the extent to which physiological responses influence cloud cover in these regions (discussed in 3.4.2).

3.4. Mechanisms of Physiologically-Driven Warming

3.4.1. Mechanisms over Land

The physiological effect increases near-surface air temperatures over land by modifying surface properties which modulate terrestrial energy fluxes (Bonan 2008; Laguë et al. 2019). This occurs through (1) changes in the partitioning between surface turbulent fluxes resulting from physiological influences on evapotranspiration, (2) radiative changes due to physiologically-driven changes in albedo, cloud cover, and column water vapor, and (3) changes in surface roughness resulting from changes in leaf area and vegetation distribution.

In most models, plants' response to CO_2 causes a net decrease in mean land evapotranspiration, especially in the tropics (Figure 6), indicating that stomatal closure decreases evapotranspiration by enough to offset increases in evapotranspiration from increased leaf area, though the magnitude and sign of evapotranspiration change does vary spatially across models. In the CMIP6 multi-model mean at $2xCO_2$, global leaf area changes increase evapotranspiration by 0.19 mm/day (σ: 0.17 mm/day; range: 0.00-0.52 mm/day), changes in stomatal conductance (approximated by the change in transpiration per leaf area) decrease global land evapotranspiration by 0.13 mm/day (σ: 0.10 mm/day; range: 0.00-0.29 mm/day), and the interaction between changes in stomatal conductance and leaf area decreases evapotranspiration by an additional 0.08 mm/day (σ: 0.10 mm/day; range: 0.00-0.29 mm/day; Figure 6c). Land evaporation changes minimally (0.01 mm/day; σ: 0.03 mm/day; range: -0.06 - +0.06 mm/day;

Figure 6c). In the multi-model mean, the net effect of these physiological responses is a decrease in evapotranspiration, with the largest and most robust decrease in the tropics (Figures 6). This physiologically-driven decrease in evapotranspiration due to increased CO_2 has previously been documented for CMIP5 models (Swann et al. 2016; Lemordant et al. 2018), and holds for the new CMIP6 models analyzed here. Under constant net radiation at the surface, this physiologically-driven decrease in evapotranspiration results in more energy leaving the land surface through sensible heating (Figure 7), thereby increasing near-surface air temperatures.

The physiological effect also increases surface and near-surface temperatures by generally increasing the net radiation at the surface (Figure 7l). Net shortwave radiation on land increases primarily through decreases in albedo and cloud cover (Figure 7d). Albedo decreases primarily in high latitudes (Figure 6), due to both increases in leaf area and decreases in snow cover due to increased temperatures. Consistent with previous studies (Doutriaux-Boucher et al. 2009; Andrews et al. 2011, 2012; Arellano et al. 2012; Lemordant et al. 2018), downwelling shortwave radiation (SW_{down}) reaching the surface also increases as a consequence of decreases in cloud cover (especially in Northern Hemisphere mid- and high-latitudes and over the northeastern Amazon; Figure 7b), which are driven both by decreases in relative humidity from physiologically-forced reductions in evapotranspiration and by increases in air temperature. In the multi-model mean, the physiological effect causes only modest changes in clear-sky SW_{down} (Figure 7), though some individual models do show significant SW_{down} changes, which could be modified by changes in water vapor and aerosols (e.g., as Andrews et al. 2012 documented in HadGEM2-ES due to vegetation's influence on dust optical depth).

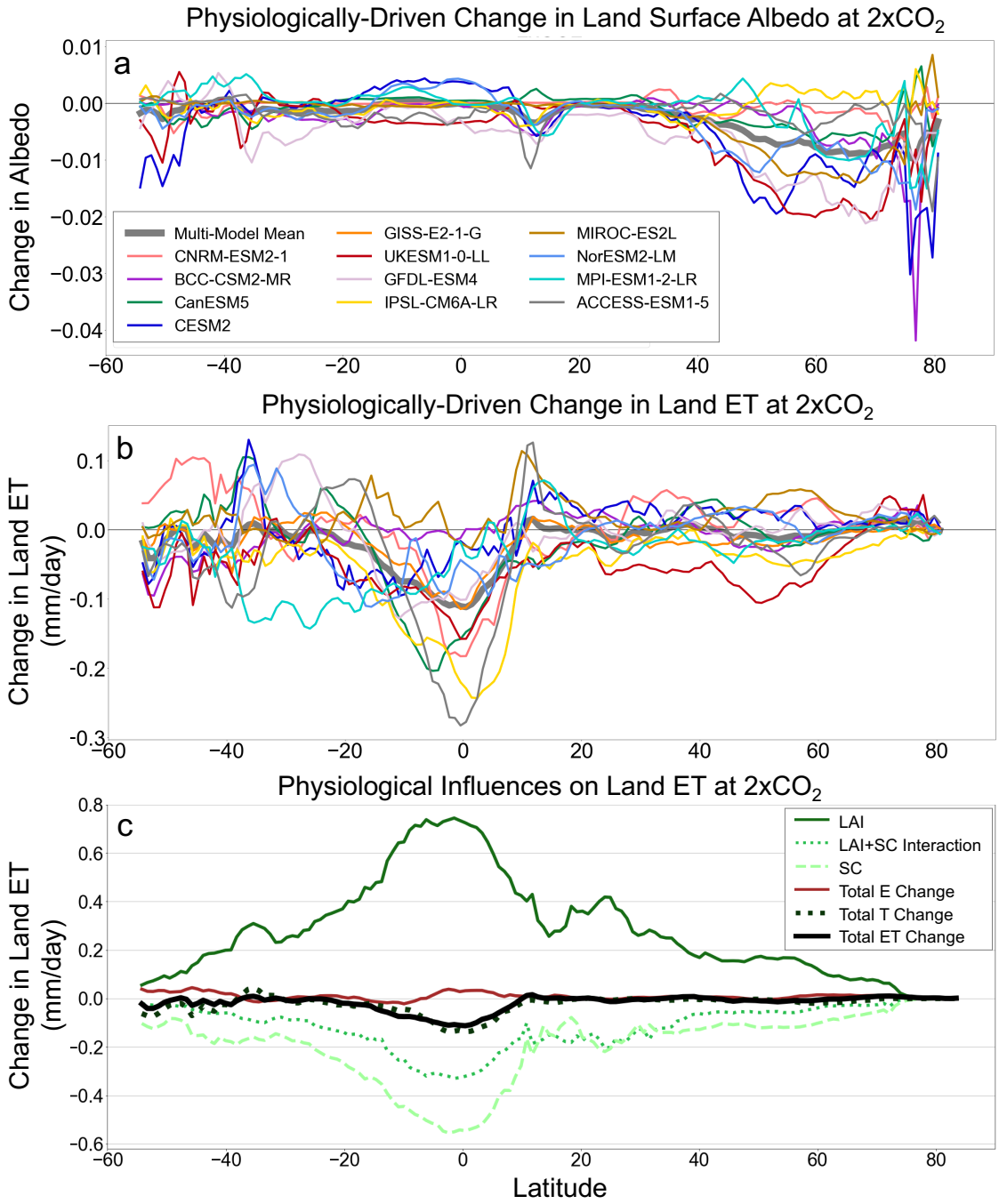

Figure 6. Land zonal means of physiologically-driven changes in (a) land surface albedo and (b) evapotranspiration at 2xCO_2 for CMIP6 models, as calculated by FULL-RAD. (c) Zonal means of how much physiologically-driven changes in different land processes (LAI, stomatal conductance, and evaporation) contribute to the total multi-model mean physiologically-driven change in land evapotranspiration, where the partitioning is calculated with Equation 1. Multi-model means in this figure are averaged across all CMIP6 models for which model output is available, which consists of up to 12 models. Transpiration and LAI data necessary for this partitioning were not available for GFDL-ESM4, MPI-ESM1-2-LR, and ACCESS-ESM1-5 so these models are only included in the multi-model mean for the total evapotranspiration change.

.

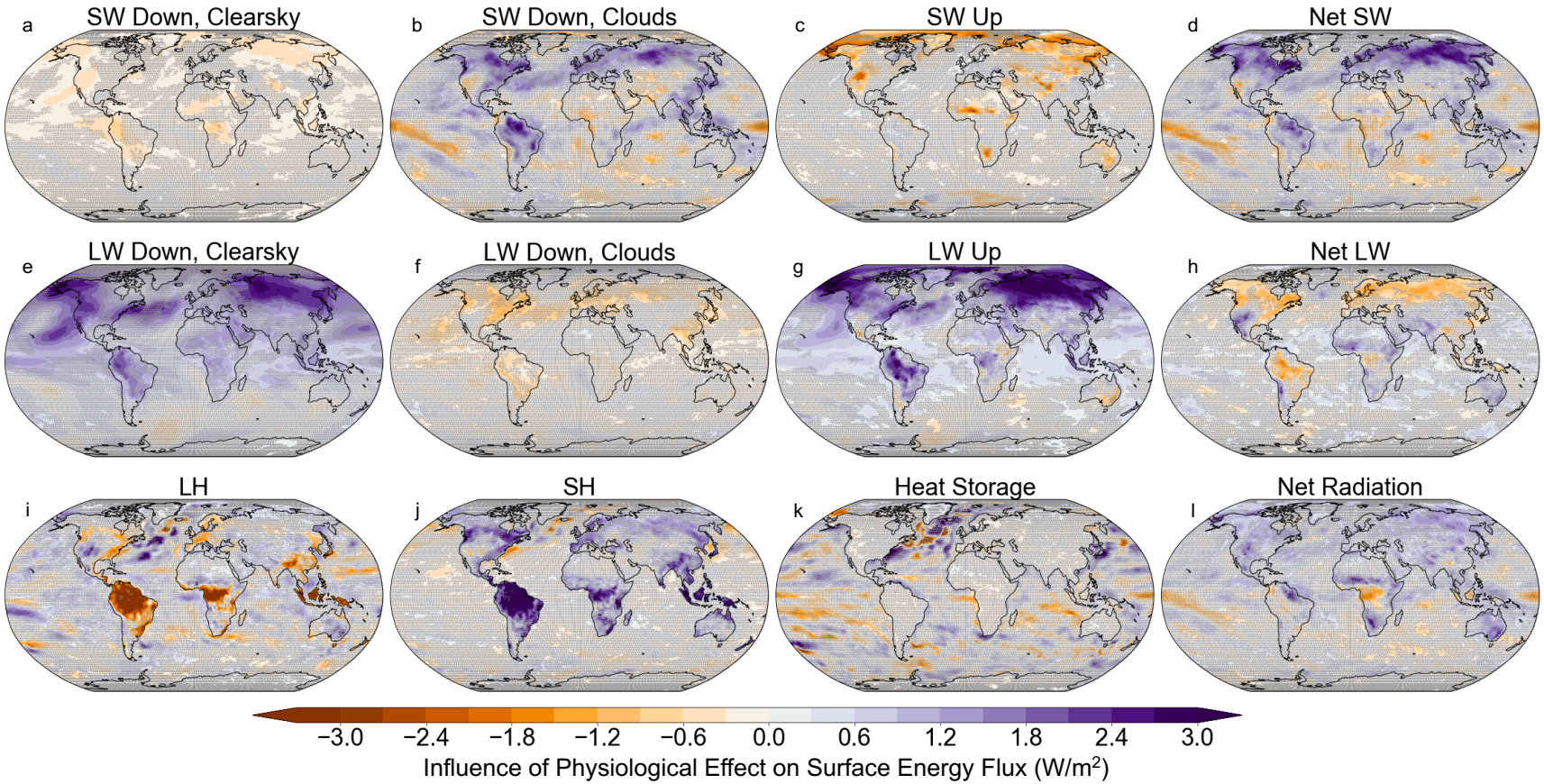

Figure 7. Spatial pattern of multi-model mean physiologically-driven changes in surface energy fluxes as calculated by FULL-RAD at the point of CO_2 doubling (averaged over years 61-80) for (a) clear-sky downwelling shortwave radiation, (b) cloudy downwelling shortwave radiation, (c) upwelling shortwave radiation, (d) net shortwave radiation, (e) clear-sky downwelling longwave radiation, (f) cloudy downwelling longwave radiation, (g) upwelling longwave radiation, (h) net longwave radiation, (i) latent heat (LH), (j) sensible heat (SH), (k) heat uptake (G), and (l) net radiation (R_{net}). Because the surface energy budget is balanced, LH + SH + G = R_{net}. The cloudy radiative fluxes in (b) and (e) are calculated as the difference between all-sky and clear-sky radiative fluxes. Multi-model means include all CMIP6 models for which model output is available; this consists of up to 12 models. Data for some surface energy fluxes were not available for the following models: GFDL-ESM4 (panels a, b, d, and f), GISS-E2-1-G, 3 (panels c and j) and CNRM-ESM2-1 (panels e and f). Stippling indicates regions where less than 8 models agree on the sign of change.

The physiological effect also influences surface net longwave radiation (Figure 7h) through changes in surface and boundary layer temperatures, cloud cover, atmospheric column water vapor, and the partitioning of surface energy fluxes. Outgoing longwave radiation from the land surface (LW_{up}) increases with increasing surface temperature through the Planck feedback (Figure 7g). This increase in LW_{up} is partially offset by increases in clear-sky downward longwave radiation at the land surface (LW_{down}; Figure 7e). Clear-sky LW_{down} increases due to warming of the boundary layer driven by both increased sensible heating and by longwave radiation associated with surface warming (Vargas Zeppetello et al. 2019), and clear-sky LW_{down} can also be influenced by physiologically-driven changes in atmospheric water vapor. Cloud changes resulting from reduced land evapotranspiration decrease LW_{down} (Figure 7f). The net effect of all of these processes generally results in a decrease of net longwave radiation over most vegetated land (Figure 7h).

3.4.2. Mechanisms over Ocean

Because most models do not have any mechanism through which ocean carbon cycle responses to CO_2 can influence ocean temperatures, the modeled oceanic warming as calculated by FULL-RAD must be the result of remote, land-driven warming. Recognizing the oceanic component of physiologically-driven warming is important because it constitutes about half of TCR_{PHYS} – even though the magnitude of physiologically-driven oceanic warming is much smaller than land warming on a per area basis, the TCR is a global-scale metric and ocean constitutes about 70% of the Earth's surface area.

The physiological effect on land can alter ocean temperatures through advection of continental air that has been directly influenced by changes in land surface properties (e.g. changes in air temperature or moisture content) as well as through changes in atmospheric or

oceanic circulation. Some robust oceanic warming regions are downwind of warming land regions, which could be associated with advection of warm continental air by the prevailing winds. Cloud cover over oceans also decreases in some regions that are downwind of land, particularly in the North Atlantic, increasing ocean temperatures by increasing net radiation (Figure 7). Teleconnections likely also contribute to ocean warming, based on past work indicating that changes in large-scale atmospheric circulation and atmospheric energy transport can be induced by physiological forcing (Kooperman et al. 2018a; Langenbrunner et al. 2019; Saint-Lu et al. 2019; Park et al. 2020) or other changes in land surface properties (Swann et al. 2012, 2014; Devaraju et al. 2015; Laguë and Swann 2016; Devaraju et al. 2018). Additionally, the physiological effect has the potential to induce changes in ocean circulation (e.g., Diffenbaugh et al. 2004). Exploration of the links between land surface perturbations and ocean temperature merits further research.

Chapter 4.
DISCUSSION AND IMPLICATIONS

4.1. Magnitude of the Physiological Contribution to the TCR

The biological and ecological processes governing canopy leaf area and stomatal conductance are often considered to exist squarely in the domain of carbon cycle feedbacks (i.e., they impact the climate system through their influence on CO_2 concentrations themselves). Our analysis demonstrates that these terrestrial carbon cycle processes are also embedded in global climate sensitivity metrics like the TCR through plants' impact on land surface properties and surface energy fluxes.

We quantified the plant physiological effect's small but significant influence on CO_2-forced temperature changes, finding that at $2xCO_2$ the physiological effect contributes about 0.12°C (6.1%) to the TCR and leads to about 0.22°C of warming over non-glaciated land. Recognizing this physiological component of CO_2 forcing is necessary for understanding forcing differences across greenhouse gases (e.g. increasing N_2O concentration does not induce warming from physiological responses) and has implications for estimating the TCR from historical observations. Because some of the observed historical temperature change has been driven by non-CO_2 forcing agents which do not induce physiological responses in plants, estimates of the TCR from historical observations may be biased low, though this is likely a small effect since CO_2 currently constitutes the majority of the total radiative forcing. While the physiological effect can constitute over 10% of the total TCR in some CMIP6 models, changes in the representation of plant physiology do not appear to be a driver of the increase in the TCR observed from CMIP5 to CMIP6.

The significant physiologically-driven warming at higher CO_2 concentrations, inter-model agreement in the sign of TCR_{PHYS}, and consistent spatial pattern of warming gives us confidence that we are detecting a real physiologically-driven signal and not just a residual from internal variability. However, internal variability is a large source of uncertainty in quantifying TCR_{PHYS} (Figure 1c), and this uncertainty is intrinsically included in estimates of TCR_{FULL}. Integration of a large-ensembles approach into the next C4MIP is necessary to address this issue and to reduce uncertainties in the TCR in future work (Deser et al. 2020). This could be done through integrating a requirement for a minimum number of initial condition ensembles in the experiment.

A limitation of our study is that the C4MIP model output necessary to disentangle physiologically- and radiatively-forced warming is only available for about a quarter of the models for which we can estimate the full TCR (12 of 47 for CMIP6 and 8 of 30 for CMIP5). We therefore cannot quantify TCR_{PHYS}, or the physiological contribution to uncertainty in the TCR, for the remaining CMIP models. Future work could further leverage C4MIP model output to assess whether signatures of physiologically-driven warming (such as seasonal variations in the CO_2-forced change of the diurnal temperature range; Bounoua et al. 1999; Collatz et al. 2000) could be used to estimate the physiological contributions to mean warming from the FULL experiments alone.

4.2. Broad Implications of Carbon Cycle Uncertainty

The terrestrial carbon cycle's influence on global warming means that uncertainty in terrestrial carbon cycle processes contributes to uncertainty in CO_2-forced warming. We find that in CMIP6, the physiological effect explains about 13.6% of the standard deviation in CO_2-forced warming over non-glaciated land. We also identify several forested land regions (tropical Africa,

northwestern South America, and the southeastern United States) for which the physiological effect contributes as much as the radiative effect (i.e. about 50% of the total) to inter-model disagreement in local warming at 2xCO_2. The spread in the magnitude of physiologically-driven warming across CMIP6 models represents real scientific uncertainty, as there are limited observational constraints to suggest that either the high or low extremes of modeled physiological responses of stomatal conductance, leaf area, and resulting evapotranspiration are within expectations (Medlyn et al. 2011; De Kauwe et al. 2013; Schimel et al. 2015).

It is also possible that ESMs do not probe the full scientific uncertainty surrounding plants' responses to CO_2, as models may contain systematic biases. For example, many models represent stomatal conductance using the same key parameters (e.g., the same slope constant in the Ball-Berry (1987) stomatal conductance model or the g1 fitted parameter in the Medlyn (2011) model) to govern how stomatal conductance responds to increasing CO_2, despite the wide variation in these parameters across and within plant functional types (Lin et al. 2015; Wolz et al. 2017). Similarly, some studies suggest (e.g. Smith et al. 2016) that ESMs systematically overestimate the leaf area increases resulting from CO_2 fertilization, which would mean that models overestimate physiologically-driven albedo decreases and underestimate physiologically-driven evapotranspiration decreases. We would expect this to result in a true physiologically-forced temperature change that is smaller than models suggest at high latitudes (where albedo matters more) and larger than models suggest at low latitudes (where ET matters more). Furthermore, Green et al. (2017) suggest that ESMs may systematically underestimate some feedbacks between land biosphere changes and the atmosphere.

On the one hand, acknowledging the physiological contribution to uncertainty in modeled CO_2-forced warming suggests that models agree more on the magnitude of radiatively forced

warming than the prevailing narrative implies. For atmospheric dynamicists most interested in purely radiatively-driven processes, these findings therefore motivate more deliberate consideration of plant functioning in experimental designs; RAD simulations may be more appropriate than FULL simulations for some climate dynamics questions. On the other hand, acknowledging the physiological contribution means that reducing uncertainty in the full (Earth System) TCR requires reducing uncertainty in land surface processes which are especially difficult to constrain. From this perspective, these findings provide a new motivation for further experimental studies to reduce uncertainty in terrestrial carbon cycle processes. For example, we identify that plants' responses to CO_2 are a major driver of uncertainty in transient warming in tropical Africa, and no free-air CO_2 enrichment (FACE) experiments exist in tropical forests to constrain uncertainty in how those ecosystems will respond to increasing CO_2.

Additionally, while this study focuses on how the physiological effect influences temperature and the TCR, uncertainty surrounding plant physiological responses to CO_2 can influence many aspects of the climate system. Because plant physiological responses affect land evapotranspiration, uncertainty surrounding plant physiological responses propagates to uncertainty in the hydrologic cycle. Previous studies have demonstrated that plant physiological responses play a critical role in determining the influence of increasing CO_2 concentration on runoff (Kooperman et al. 2018b) and precipitation (Kooperman et al. 2018a; Chadwick et al. 2017, 2019), especially in the Amazon (Richardson et al. 2018; Langenbrunner et al. 2019). Our finding that plant physiology contributes to inter-model variation in CO_2-forced warming could therefore motivate further analyses of RAD and PHYS experiments to quantify the physiological contribution to uncertainty in these quantities. Carbon cycle uncertainty is not limited to the

carbon cycle, and efforts to reduce uncertainty in plants' responses to CO_2 will also help to reduce uncertainty in the physical climate response to increasing CO_2.

BIBLIOGRAPHY

Anav, A., and Coauthors, 2013: Evaluating the Land and Ocean Components of the Global Carbon Cycle in the CMIP5 Earth System Models. *J. Clim.*, **26**, https://doi.org/10.1175/JCLI-D-12-00417.1.

Andrews, T., P. M. Forster, and J. M. Gregory, 2009: A Surface Energy Perspective on Climate Change. *J. Clim.*, **22**, 2557–2570, https://doi.org/10.1175/2008JCLI2759.1.

——, M. Doutriaux-Boucher, O. Boucher, and P. M. Forster, 2011: A regional and global analysis of carbon dioxide physiological forcing and its impact on climate. *Clim. Dyn.*, **36**, 783–792, https://doi.org/10.1007/s00382-010-0742-1.

——, M. A. Ringer, M. Doutriaux-Boucher, M. J. Webb, and W. J. Collins, 2012: Sensitivity of an Earth system climate model to idealized radiative forcing. *Geophys. Res. Lett.*, **39**, https://doi.org/10.1029/2012GL051942.

——, and Coauthors, 2019: Forcings, Feedbacks, and Climate Sensitivity in HadGEM3-GC3.1 and UKESM1. *J. Adv. Model. Earth Syst.*, **n/a**, https://doi.org/10.1029/2019MS001866.

Arellano, J. V.-G. de, C. C. van Heerwaarden, and J. Lelieveld, 2012: Modelled suppression of boundary-layer clouds by plants in a CO 2 -rich atmosphere. *Nat. Geosci.*, **5**, 701–704, https://doi.org/10.1038/ngeo1554.

Arora, V. K., and G. J. Boer, 2010: Uncertainties in the 20th century carbon budget associated with land use change. *Glob. Change Biol.*, **16**, 3327–3348, https://doi.org/10.1111/j.1365-2486.2010.02202.x.

——, and Coauthors, 2009: The Effect of Terrestrial Photosynthesis Down Regulation on the Twentieth-Century Carbon Budget Simulated with the CCCma Earth System Model. *J. Clim.*, **22**, 6066–6088, https://doi.org/10.1175/2009JCLI3037.1.

——, and Coauthors, 2011: Carbon emission limits required to satisfy future representative concentration pathways of greenhouse gases. *Geophys. Res. Lett.*, **38**, https://doi.org/10.1029/2010GL046270.

Arora, V. K., and Coauthors, 2013: Carbon–Concentration and Carbon–Climate Feedbacks in CMIP5 Earth System Models. *J. Clim.*, **26**, 5289–5314, https://doi.org/10.1175/JCLI-D-12-00494.1.

——, and Coauthors, 2019: Carbon-concentration and carbon-climate feedbacks in CMIP6 models, and their comparison to CMIP5 models. *Biogeosciences Discuss.*, https://doi.org/10.5194/bg-2019-473.

Bala, G., K. Caldeira, A. Mirin, M. Wickett, C. Delire, and T. J. Phillips, 2006: Biogeophysical effects of CO2 fertilization on global climate. *Tellus B*, **58**, 620–627, https://doi.org/10.1111/j.1600-0889.2006.00210.x.

Ball, J. T., I. E. Woodrow, and J. A. Berry, 1987: A Model Predicting Stomatal Conductance and its Contribution to the Control of Photosynthesis under Different Environmental Conditions. *Progress in Photosynthesis Research*, J. Biggins, Ed., Springer Netherlands, 221–224.

Bentsen, M., and Coauthors, 2013: The Norwegian Earth System Model, NorESM1-M – Part 1: Description and basic evaluation of the physical climate. *Geosci. Model Dev.*, **6**, 687–720, https://doi.org/10.5194/gmd-6-687-2013.

Betts, R. A., 2000: Offset of the potential carbon sink from boreal forestation by decreases in surface albedo. *Nature*, **408**, 187–190, https://doi.org/10.1038/35041545.

——, P. M. Cox, S. E. Lee, and F. I. Woodward, 1997: Contrasting physiological and structural vegetation feedbacks in climate change simulations. *Nature*, **387**, 796–799, https://doi.org/10.1038/42924.

——, and Coauthors, 2007: Projected increase in continental runoff due to plant responses to increasing carbon dioxide. *Nature*, **448**, 1037–1041, https://doi.org/10.1038/nature06045.

Bonan, G. B., 2008: Forests and Climate Change: Forcings, Feedbacks, and the Climate Benefits of Forests. *Science*, **320**, 1444–1449, https://doi.org/10.1126/science.1155121.

Boucher, O., A. Jones, and R. A. Betts, 2009: Climate response to the physiological impact of carbon dioxide on plants in the Met Office Unified Model HadCM3. *Clim. Dyn.*, **32**, 237–249, https://doi.org/10.1007/s00382-008-0459-6.

Bounoua, L., and Coauthors, 1999: Interactions between Vegetation and Climate: Radiative and Physiological Effects of Doubled Atmospheric CO2. *J. Clim.*, **12**, 309–324, https://doi.org/10.1175/1520-0442(1999)012<0309:IBVACR>2.0.CO;2.

——, F. G. Hall, P. J. Sellers, A. Kumar, G. J. Collatz, C. J. Tucker, and M. L. Imhoff, 2010: Quantifying the negative feedback of vegetation to greenhouse warming: A modeling approach. *Geophys. Res. Lett.*, **37**, https://doi.org/10.1029/2010GL045338.

Byrne, M. P., and P. A. O'Gorman, 2016: Understanding Decreases in Land Relative Humidity with Global Warming: Conceptual Model and GCM Simulations. *J. Clim.*, **29**, 9045–9061, https://doi.org/10.1175/JCLI-D-16-0351.1.

——, and ——, 2018: Trends in continental temperature and humidity directly linked to ocean warming. *Proc. Natl. Acad. Sci.*, **115**, 4863–4868, https://doi.org/10.1073/pnas.1722312115.

Cao, L., G. Bala, K. Caldeira, R. Nemani, and G. Ban-Weiss, 2009: Climate response to physiological forcing of carbon dioxide simulated by the coupled Community Atmosphere Model (CAM3.1) and Community Land Model (CLM3.0). *Geophys. Res. Lett.*, **36**, https://doi.org/10.1029/2009GL037724.

——, ——, ——, ——, and G. Ban-Weiss, 2010: Importance of carbon dioxide physiological forcing to future climate change. *Proc. Natl. Acad. Sci.*, **107**, 9513–9518, https://doi.org/10.1073/pnas.0913000107.

Chadwick, R., H. Douville, and C. B. Skinner, 2017: Timeslice experiments for understanding regional climate projections: applications to the tropical hydrological cycle and European winter circulation. *Clim. Dyn.*, **49**, 3011–3029, https://doi.org/10.1007/s00382-016-3488-6.

——, D. Ackerley, T. Ogura, and D. Dommenget, 2019: Separating the Influences of Land Warming, the Direct CO2 Effect, the Plant Physiological Effect, and SST Warming on

Regional Precipitation Changes. *J. Geophys. Res. Atmospheres*, **124**, 624–640, https://doi.org/10.1029/2018JD029423.

Collatz, G. J., L. Bounoua, S. O. Los, D. A. Randall, I. Y. Fung, and P. J. Sellers, 2000: A mechanism for the influence of vegetation on the response of the diurnal temperature range to changing climate. *Geophys. Res. Lett.*, **27**, 3381–3384, https://doi.org/10.1029/1999GL010947.

Collins, W. J., and Coauthors, 2011: Development and evaluation of an Earth-System model – HadGEM2. *Geosci. Model Dev.*, **4**, 1051–1075, https://doi.org/10.5194/gmd-4-1051-2011.

Cox, P. M., R. A. Betts, C. B. Bunton, R. L. H. Essery, P. R. Rowntree, and J. Smith, 1999: The impact of new land surface physics on the GCM simulation of climate and climate sensitivity. *Clim. Dyn.*, **15**, 183–203, https://doi.org/10.1007/s003820050276.

Danabasoglu, G., and Coauthors, The Community Earth System Model version 2 (CESM2). *J. Adv. Model. Earth Syst.*, **n/a**, e2019MS001916, https://doi.org/10.1029/2019MS001916.

De Kauwe, M. G., and Coauthors, 2013: Forest water use and water use efficiency at elevated CO2: a model-data intercomparison at two contrasting temperate forest FACE sites. *Glob. Change Biol.*, **19**, 1759–1779, https://doi.org/10.1111/gcb.12164.

Decharme, B., and Coauthors, 2019: Recent Changes in the ISBA-CTRIP Land Surface System for Use in the CNRM-CM6 Climate Model and in Global Off-Line Hydrological Applications. *J. Adv. Model. Earth Syst.*, **11**, 1207–1252, https://doi.org/10.1029/2018MS001545.

Deser, C., and Coauthors, 2020: Insights from Earth system model initial-condition large ensembles and future prospects. *Nat. Clim. Change*, **10**, 277–286, https://doi.org/10.1038/s41558-020-0731-2.

Devaraju, N., G. Bala, and A. Modak, 2015: Effects of large-scale deforestation on precipitation in the monsoon regions: Remote versus local effects. *Proc. Natl. Acad. Sci.*, **112**, 3257–3262, https://doi.org/10.1073/pnas.1423439112.

——, N. de Noblet-Ducoudré, B. Quesada, and G. Bala, 2018: Quantifying the Relative Importance of Direct and Indirect Biophysical Effects of Deforestation on Surface Temperature and Teleconnections. *J. Clim.*, **31**, 3811–3829, https://doi.org/10.1175/JCLI-D-17-0563.1.

Diffenbaugh, N. S., M. A. Snyder, and L. C. Sloan, 2004: Could CO2-induced land-cover feedbacks alter near-shore upwelling regimes? *Proc. Natl. Acad. Sci.*, **101**, 27–32, https://doi.org/10.1073/pnas.0305746101.

Dong, B., J. M. Gregory, and R. T. Sutton, 2009: Understanding Land–Sea Warming Contrast in Response to Increasing Greenhouse Gases. Part I: Transient Adjustment. *J. Clim.*, **22**, 3079–3097, https://doi.org/10.1175/2009JCLI2652.1.

Donohue, R. J., M. L. Roderick, T. R. McVicar, and G. D. Farquhar, 2013: Impact of CO2 fertilization on maximum foliage cover across the globe's warm, arid environments. *Geophys. Res. Lett.*, **40**, 3031–3035, https://doi.org/10.1002/grl.50563.

Doutriaux-Boucher, M., M. J. Webb, J. M. Gregory, and O. Boucher, 2009: Carbon dioxide induced stomatal closure increases radiative forcing via a rapid reduction in low cloud. *Geophys. Res. Lett.*, **36**, https://doi.org/10.1029/2008GL036273.

Douville, H., S. Planton, J.-F. Royer, D. B. Stephenson, S. Tyteca, L. Kergoat, S. Lafont, and R. A. Betts, 2000: Importance of vegetation feedbacks in doubled-CO2 climate experiments. *J. Geophys. Res. Atmospheres*, **105**, 14841–14861, https://doi.org/10.1029/1999JD901086.

Dufresne, J.-L., and Coauthors, 2013: Climate change projections using the IPSL-CM5 Earth System Model: from CMIP3 to CMIP5. *Clim. Dyn.*, **40**, 2123–2165, https://doi.org/10.1007/s00382-012-1636-1.

Dunne, J. P., and Coauthors, 2012: GFDL's ESM2 Global Coupled Climate–Carbon Earth System Models. Part I: Physical Formulation and Baseline Simulation Characteristics. *J. Clim.*, **25**, 6646–6665, https://doi.org/10.1175/JCLI-D-11-00560.1.

Field, C. B., R. B. Jackson, and H. A. Mooney, 1995: Stomatal responses to increased CO2: implications from the plant to the global scale. *Plant Cell Environ.*, **18**, 1214–1225, https://doi.org/10.1111/j.1365-3040.1995.tb00630.x.

Flynn, C. M., and T. Mauritsen, 2020: On the Climate Sensitivity and Historical Warming Evolution in Recent Coupled Model Ensembles. *Atmospheric Chem. Phys. Discuss.*, https://doi.org/10.5194/acp-2019-1175.

Friedlingstein, P., and Coauthors, 2006: Climate–Carbon Cycle Feedback Analysis: Results from the C4MIP Model Intercomparison. *J. Clim.*, **19**, 3337–3353, https://doi.org/10.1175/JCLI3800.1.

Gettelman, A., and Coauthors, 2019: High Climate Sensitivity in the Community Earth System Model Version 2 (CESM2). *Geophys. Res. Lett.*, **46**, 8329–8337, https://doi.org/10.1029/2019GL083978.

Giorgetta, M. A., and Coauthors, 2013: Climate and carbon cycle changes from 1850 to 2100 in MPI-ESM simulations for the Coupled Model Intercomparison Project phase 5. *J. Adv. Model. Earth Syst.*, **5**, 572–597, https://doi.org/10.1002/jame.20038.

Golaz, J.-C., and Coauthors, 2019: The DOE E3SM Coupled Model Version 1: Overview and Evaluation at Standard Resolution. *J. Adv. Model. Earth Syst.*, **11**, 2089–2129, https://doi.org/10.1029/2018MS001603.

Goosse, H., and Coauthors, 2018: Quantifying climate feedbacks in polar regions. *Nat. Commun.*, **9**, 1919, https://doi.org/10.1038/s41467-018-04173-0.

Green, J. K., A. G. Konings, S. H. Alemohammad, J. Berry, D. Entekhabi, J. Kolassa, J.-E. Lee, and P. Gentine, 2017: Regionally strong feedbacks between the atmosphere and terrestrial biosphere. *Nat. Geosci.*, **10**, 410–414, https://doi.org/10.1038/ngeo2957.

Gregory, J. M., and P. M. Forster, 2008: Transient climate response estimated from radiative forcing and observed temperature change. *J. Geophys. Res. Atmospheres*, **113**, https://doi.org/10.1029/2008JD010405.

——, T. Andrews, and P. Good, 2015: The inconstancy of the transient climate response parameter under increasing CO2. *Philos. Trans. R. Soc. Math. Phys. Eng. Sci.*, **373**, 20140417, https://doi.org/10.1098/rsta.2014.0417.

Grose, M. R., J. Gregory, R. Colman, and T. Andrews, 2018: What Climate Sensitivity Index Is Most Useful for Projections? *Geophys. Res. Lett.*, **45**, 1559–1566, https://doi.org/10.1002/2017GL075742.

Hajima, T., and Coauthors, Submitted: Description of the MIROC-ES2L Earth system model and evaluation of its climate–biogeochemical processes and feedbacks. *Geosci. Model Dev. Discuss.*, 1–73, https://doi.org/10.5194/gmd-2019-275.

Hense, I., I. Stemmler, and S. Sonntag, 2017: Ideas and perspectives: climate-relevant marine biologically driven mechanisms in Earth system models. *Biogeosciences*, **14**, 403–413, https://doi.org/10.5194/bg-14-403-2017.

Hungate, B. A., M. Reichstein, P. Dijkstra, D. Johnson, G. Hymus, J. D. Tenhunen, C. R. Hinkle, and B. G. Drake, 2002: Evapotranspiration and soil water content in a scrub-oak woodland under carbon dioxide enrichment. *Glob. Change Biol.*, **8**, 289–298, https://doi.org/10.1046/j.1365-2486.2002.00468.x.

Hurrell, J. W., and Coauthors, 2013: The Community Earth System Model: A Framework for Collaborative Research. *Bull. Am. Meteorol. Soc.*, **94**, 1339–1360, https://doi.org/10.1175/BAMS-D-12-00121.1.

Ito, A., and M. Inatomi, 2011: Water-Use Efficiency of the Terrestrial Biosphere: A Model Analysis Focusing on Interactions between the Global Carbon and Water Cycles. *J. Hydrometeorol.*, **13**, 681–694, https://doi.org/10.1175/JHM-D-10-05034.1.

Iversen, T., and Coauthors, 2013: The Norwegian Earth System Model, NorESM1-M – Part 2: Climate response and scenario projections. *Geosci. Model Dev.*, **6**, 389–415, https://doi.org/10.5194/gmd-6-389-2013.

Jones, C. D., and Coauthors, 2016: C4MIP -- The Coupled Climate–Carbon Cycle Model Intercomparison Project: experimental protocol for CMIP6. *Geosci. Model Dev.*, **9**, 2853–2880, https://doi.org/10.5194/gmd-9-2853-2016.

Joshi, M. M., J. M. Gregory, M. J. Webb, D. M. H. Sexton, and T. C. Johns, 2008: Mechanisms for the land/sea warming contrast exhibited by simulations of climate change. *Clim. Dyn.*, **30**, 455–465, https://doi.org/10.1007/s00382-007-0306-1.

Kim, J. E., M. M. Laguë, S. Pennypacker, E. Dawson, and A. L. S. Swann, 2020: Evaporative Resistance is of Equal Importance as Surface Albedo in High-Latitude Surface Temperatures Due to Cloud Feedbacks. *Geophys. Res. Lett.*, **47**, e2019GL085663, https://doi.org/10.1029/2019GL085663.

Kooperman, G. J., Y. Chen, F. M. Hoffman, C. D. Koven, K. Lindsay, M. S. Pritchard, A. L. S. Swann, and J. T. Randerson, 2018a: Forest response to rising CO2 drives zonally asymmetric rainfall change over tropical land. *Nat. Clim. Change*, **8**, 434–440, https://doi.org/10.1038/s41558-018-0144-7.

——, M. D. Fowler, F. M. Hoffman, C. D. Koven, K. Lindsay, M. S. Pritchard, A. L. S. Swann, and J. T. Randerson, 2018b: Plant Physiological Responses to Rising CO2 Modify

Simulated Daily Runoff Intensity With Implications for Global-Scale Flood Risk Assessment. *Geophys. Res. Lett.*, **45**, 12,457-12,466, https://doi.org/10.1029/2018GL079901.

Laguë, M. M., and A. L. S. Swann, 2016: Progressive Midlatitude Afforestation: Impacts on Clouds, Global Energy Transport, and Precipitation. *J. Clim.*, **29**, 5561–5573, https://doi.org/10.1175/JCLI-D-15-0748.1.

——, G. B. Bonan, and A. L. S. Swann, 2019: Separating the Impact of Individual Land Surface Properties on the Terrestrial Surface Energy Budget in both the Coupled and Uncoupled Land–Atmosphere System. *J. Clim.*, **32**, 5725–5744, https://doi.org/10.1175/JCLI-D-18-0812.1.

Langenbrunner, B., M. S. Pritchard, G. J. Kooperman, and J. T. Randerson, 2019: Why Does Amazon Precipitation Decrease When Tropical Forests Respond to Increasing CO2? *Earths Future*, **7**, 450–468, https://doi.org/10.1029/2018EF001026.

Lawrence, D. M., and Coauthors, 2011: Parameterization improvements and functional and structural advances in Version 4 of the Community Land Model. *J. Adv. Model. Earth Syst.*, **3**, https://doi.org/10.1029/2011MS00045.

——, and Coauthors, 2019: The Community Land Model Version 5: Description of New Features, Benchmarking, and Impact of Forcing Uncertainty. *J. Adv. Model. Earth Syst.*, **11**, 4245–4287, https://doi.org/10.1029/2018MS001583.

Leakey, A. D. B., E. A. Ainsworth, C. J. Bernacchi, A. Rogers, S. P. Long, and D. R. Ort, 2009: Elevated CO2 effects on plant carbon, nitrogen, and water relations: six important lessons from FACE. *J. Exp. Bot.*, **60**, 2859–2876, https://doi.org/10.1093/jxb/erp096.

Lemordant, L., and P. Gentine, 2019: Vegetation Response to Rising CO2 Impacts Extreme Temperatures. *Geophys. Res. Lett.*, **46**, 1383–1392, https://doi.org/10.1029/2018GL080238.

——, ——, M. Stéfanon, P. Drobinski, and S. Fatichi, 2016: Modification of land-atmosphere interactions by CO2 effects: Implications for summer dryness and heat wave amplitude. *Geophys. Res. Lett.*, **43**, 10,240-10,248, https://doi.org/10.1002/2016GL069896.

——, ——, A. S. Swann, B. I. Cook, and J. Scheff, 2018: Critical impact of vegetation physiology on the continental hydrologic cycle in response to increasing CO2. *Proc. Natl. Acad. Sci.*, **115**, 4093–4098, https://doi.org/10.1073/pnas.1720712115.

Levis, S., J. A. Foley, and D. Pollard, 2000: Large-Scale Vegetation Feedbacks on a Doubled CO2 Climate. *J. Clim.*, **13**, 1313–1325, https://doi.org/10.1175/1520-0442(2000)013<1313:LSVFOA>2.0.CO;2.

Lian, X., and Coauthors, 2018: Partitioning global land evapotranspiration using CMIP5 models constrained by observations. *Nat. Clim. Change*, **8**, 640–646, https://doi.org/10.1038/s41558-018-0207-9.

Lin, Y.-S., and Coauthors, 2015: Optimal stomatal behaviour around the world. *Nat. Clim. Change*, **5**, 459–464, https://doi.org/10.1038/nclimate2550.

Lindsay, K., and Coauthors, 2014: Preindustrial-Control and Twentieth-Century Carbon Cycle Experiments with the Earth System Model CESM1(BGC). *J. Clim.*, **27**, 8981–9005, https://doi.org/10.1175/JCLI-D-12-00565.1.

Mahowald, N., F. Lo, Y. Zheng, L. Harrison, C. Funk, D. Lombardozzi, and C. Goodale, 2016: Projections of leaf area index in earth system models. *Earth Syst. Dyn.*, **7**, 211–229, https://doi.org/10.5194/esd-7-211-2016.

Martin, G. M., and Coauthors, 2011: The HadGEM2 family of Met Office Unified Model climate configurations. *Geosci. Model Dev.*, **4**, 723–757, https://doi.org/10.5194/gmd-4-723-2011.

Mauritsen, T., and Coauthors, 2019: Developments in the MPI-M Earth System Model version 1.2 (MPI-ESM1.2) and Its Response to Increasing CO2. *J. Adv. Model. Earth Syst.*, **11**, 998–1038, https://doi.org/10.1029/2018MS001400.

Medlyn, B. E., and Coauthors, 2011: Reconciling the optimal and empirical approaches to modelling stomatal conductance. *Glob. Change Biol.*, **17**, 2134–2144, https://doi.org/10.1111/j.1365-2486.2010.02375.x.

Norby, R. J., and D. R. Zak, 2011: Ecological Lessons from Free-Air CO2 Enrichment (FACE) Experiments. *Annu. Rev. Ecol. Evol. Syst.*, **42**, 181–203, https://doi.org/10.1146/annurev-ecolsys-102209-144647.

O'ishi, R., A. Abe-Ouchi, I. C. Prentice, and S. Sitch, 2009: Vegetation dynamics and plant CO2 responses as positive feedbacks in a greenhouse world. *Geophys. Res. Lett.*, **36**, https://doi.org/10.1029/2009GL038217.

Oleson, K. W., and Coauthors, 2010: *Technical Description of version 4.0 of the Community Land Model (CLM)*. National Center for Atmospheric Research, http://dx.doi.org/10.5065/D6FB50WZ.

Park, S.-W., J.-S. Kim, and J.-S. Kug, 2020: The intensification of Arctic warming as a result of CO 2 physiological forcing. *Nat. Commun.*, **11**, 2098, https://doi.org/10.1038/s41467-020-15924-3.

Parsons, L. A., K. M. Brennan, R. C. Jnglin Wills, and C. Proistosescu, 2020: Magnitudes and spatial patterns of interdecadal temperature variability in CMIP6. *Geophys. Res. Lett.*, **47**, https://doi.org/10.1029/2019GL086588.

Piao, S., and Coauthors, 2013: Evaluation of terrestrial carbon cycle models for their response to climate variability and to CO2 trends. *Glob. Change Biol.*, **19**, 2117–2132, https://doi.org/10.1111/gcb.12187.

Pu, B., and R. E. Dickinson, 2012: Examining vegetation feedbacks on global warming in the Community Earth System Model. *J. Geophys. Res. Atmospheres*, **117**, https://doi.org/10.1029/2012JD017623.

Qian, H., R. Joseph, and N. Zeng, 2010: Enhanced terrestrial carbon uptake in the Northern High Latitudes in the 21st century from the Coupled Carbon Cycle Climate Model Intercomparison Project model projections. *Glob. Change Biol.*, **16**, 641–656, https://doi.org/10.1111/j.1365-2486.2009.01989.x.

Richardson, T. B., and Coauthors, 2018: Carbon Dioxide Physiological Forcing Dominates Projected Eastern Amazonian Drying. *Geophys. Res. Lett.*, **45**, 2815–2825, https://doi.org/10.1002/2017GL076520.

Saint-Lu, M., R. Chadwick, F. H. Lambert, and M. Collins, 2019: Surface Warming and Atmospheric Circulation Dominate Rainfall Changes Over Tropical Rainforests Under Global Warming. *Geophys. Res. Lett.*, **46**, https://doi.org/10.1029/2019GL085295.

Schimel, D., B. B. Stephens, and J. B. Fisher, 2015: Effect of increasing CO2 on the terrestrial carbon cycle. *Proc. Natl. Acad. Sci.*, **112**, 436–441, https://doi.org/10.1073/pnas.1407302112.

Séférian, R., and Coauthors, 2019: Evaluation of CNRM Earth System Model, CNRM-ESM2-1: Role of Earth System Processes in Present-Day and Future Climate. *J. Adv. Model. Earth Syst.*, **11**, 4182–4227, https://doi.org/10.1029/2019MS001791.

Sellar, A. A., and Coauthors, 2019: UKESM1: Description and Evaluation of the U.K. Earth System Model. *J. Adv. Model. Earth Syst.*, **11**, https://doi.org/10.1029/2019MS001739.

Sellers, P. J., and Coauthors, 1996: Comparison of Radiative and Physiological Effects of Doubled Atmospheric CO2 on Climate. *Science*, **271**, 1402–1406, https://doi.org/10.1126/science.271.5254.1402.

Skinner, C. B., C. J. Poulsen, and J. S. Mankin, 2018: Amplification of heat extremes by plant CO 2 physiological forcing. *Nat. Commun.*, **9**, 1–11, https://doi.org/10.1038/s41467-018-03472-w.

Smith, W. K., S. C. Reed, C. C. Cleveland, A. P. Ballantyne, W. R. L. Anderegg, W. R. Wieder, Y. Y. Liu, and S. W. Running, 2016: Large divergence of satellite and Earth system model estimates of global terrestrial CO 2 fertilization. *Nat. Clim. Change*, **6**, 306–310, https://doi.org/10.1038/nclimate2879.

Swann, A. L. S., I. Y. Fung, and J. C. H. Chiang, 2012: Mid-latitude afforestation shifts general circulation and tropical precipitation. *Proc. Natl. Acad. Sci.*, **109**, 712–716, https://doi.org/10.1073/pnas.1116706108.

——, ——, Y. Liu, and J. C. H. Chiang, 2014: Remote Vegetation Feedbacks and the Mid-Holocene Green Sahara. *J. Clim.*, **27**, 4857–4870, https://doi.org/10.1175/JCLI-D-13-00690.1.

——, F. M. Hoffman, C. D. Koven, and J. T. Randerson, 2016: Plant responses to increasing CO2 reduce estimates of climate impacts on drought severity. *Proc. Natl. Acad. Sci.*, **113**, 10019–10024, https://doi.org/10.1073/pnas.1604581113.

Swart, N. C., and Coauthors, 2019: The Canadian Earth System Model version 5 (CanESM5.0.3). *Geosci. Model Dev.*, **12**, 4823–4873, https://doi.org/10.5194/gmd-12-4823-2019.

Tjiputra, J. F., C. Roelandt, M. Bentsen, D. M. Lawrence, T. Lorentzen, J. Schwinger, Ø. Seland, and C. Heinze, 2013: Evaluation of the carbon cycle components in the Norwegian Earth System Model (NorESM). *Geosci. Model Dev.*, **6**, 301–325, https://doi.org/10.5194/gmd-6-301-2013.

Vargas Zeppetello, L. R., A. Donohoe, and D. S. Battisti, 2019: Does Surface Temperature Respond to or Determine Downwelling Longwave Radiation? *Geophys. Res. Lett.*, **46**, 2781–2789, https://doi.org/10.1029/2019GL082220.

Wolz, K. J., T. M. Wertin, M. Abordo, D. Wang, and A. D. B. Leakey, 2017: Diversity in stomatal function is integral to modelling plant carbon and water fluxes. *Nat. Ecol. Evol.*, **1**, 1292–1298, https://doi.org/10.1038/s41559-017-0238-z.

Wu, T., and Coauthors, 2014: An overview of BCC climate system model development and application for climate change studies. *J. Meteorol. Res.*, **28**, 34–56, https://doi.org/10.1007/s13351-014-3041-7.

——, and Coauthors, 2019: The Beijing Climate Center Climate System Model (BCC-CSM): the main progress from CMIP5 to CMIP6. *Geosci. Model Dev.*, **12**, 1573–1600, https://doi.org/10.5194/gmd-12-1573-2019.

Xu, X., W. J. Riley, C. D. Koven, G. Jia, and X. Zhang, 2020: Earlier leaf-out warms air in the north. *Nat. Clim. Change*, **10**, 370–375, https://doi.org/10.1038/s41558-020-0713-4.

Appendix A.
LITERATURE REVIEW

Study Details			Experimental Setup					Processes Represented		Temperature Change (°C)		
Study	Modeling Center[1]	Model (GCM / Land Model where applicable)	CO_2 Perturbation	$1xCO_2$ (ppm)	CO_2 Level	Ocean Model[2]	Method[3]	Stom. Cond.[4]	LAI	Land	Ocean	Global
Sellers et al. (1996)	NASA / CSU	Colorado State University GCM / SiB2	Abrupt	350	2x	S	FULL-RAD	Yes	No	0.2	-	0.0
							PHYS-PI	Yes	No	0.3	-	0.1
Betts et al. (1997)	MOHC	MOHC GCM / Sheffield vegetation model	Abrupt	323	2x	S	FULL-RAD	Yes	No	0.2	-	0.2
								Yes	Yes	-0.1	-	-0.1
Cox et al. (1999)	MOHC	HadAM3 / MOSES	Abrupt	-	2x	F	FULL-RAD	Yes	No	0.39	-	-
Douville et al. (2000)	CNRM	ARPEGE-Climat / ISBA (incorporating output from HadAM3 / MOSES)	Abrupt[5]	353	2x	F[5]	FULL-RAD	Yes	No	-	-	0.04
								Yes	Yes	-	-	0.05
Levis et al. (2000)	Penn State University	GENESIS GCM / IBIS	Abrupt	345	2x	S	FULL-RAD	Yes	No	0.2	-	0.1
								Yes	Yes	0.2	-	0.1
Betts et al. (2007)	MOHC	HadSM3	Abrupt	280	2x	S	FULL-RAD	Yes	No	0.96	-	-
Cao et al. (2009)	NCAR	CAM3.1 / CLM3.0	Abrupt	355	2x	S	FULL-RAD	Yes	No	0.12	0.07	0.09
Doutriaux-Boucher et al. (2009)	MOHC	HadCM3LC	Abrupt	286	2x	-	FULL-RAD	Yes	Yes[6]	-	-	0.43
Boucher et al. (2009)	MOHC	HadCM3	Transient[7]	~346	~2x	C	FULL-RAD	Yes	No	0.52	0.14	0.25
Cao et al. (2010)	NCAR	CAM3.5 / CLM3.5	Abrupt	400	2x	S	PHYS-PI	Yes	No	0.42	0.15	0.22
							FULL-RAD	Yes	No	0.47	0.19	0.28
Pu and Dickinson (2012)	NCAR	CESM (CAM4 / CLM4)	Abrupt	367	2x	S	FULL-RAD	Yes	No	0.27	-	-
Bala et al. (2006)	LLNL	INCCA (NCAR-DOE PCTM / IBIS2)	Transient	289	~4x	C	PHYS-PI	Yes	Yes	1.41	-	0.65
O'ishi et al. (2009)	University of Tokyo, NIES, and JAMSTEC	MIROC / LPJ	Abrupt	285	4x	S	FULL-RAD	Yes	Yes	-	-	1.02
Doutriaux-Boucher et al. (2009)	MOHC	HadCM3LC	Abrupt	286	4x	-	FULL-RAD	Yes	Yes[6]	-	-	0.69
Andrews et al. (2011)	MOHC	HadCM3LC	Abrupt	286	4x	C	FULL-RAD	Yes	Yes[6]	0.82	-	0.5

TABLE A1. Summary of relevant previous work quantifying global-scale physiologically-driven warming. Studies are separated by whether they assess the physiological contribution to warming at $2xCO_2$ or $4xCO_2$, and studies are then listed chronologically. We do not include model estimates which include the effects of photosynthetic down-regulation, but Bounoua et al. (2010) suggest that down-regulation decreases physiologically-driven temperature changes while Pu and Dickinson (2012) suggest that down-regulation increases physiologically-driven temperature changes.

---

[1] Modeling center refers to the modeling center associated with the development of the model used, which does necessarily correspond to the authors' primary affiliations.
[2] S = Slab ocean model; F = fixed SSTs; C = full ocean model
[3] This column indicates whether the physiological contribution to warming was estimated by the difference between FULL and RAD simulations (FULL-RAD) or as the difference between PHYS and PI simulations (PHYS-PI). Appendix C discusses the differences between the FULL-RAD and PHYS-PI methods in more detail.
[4] Stom. Cond. = stomatal conductance
[5] $2xCO_2$ experiments used fixed SSTs obtained from a fully coupled transient experiment
[6] While LAI is allowed to respond to changing CO_2 concentrations in these studies, LAI does not respond much during the relatively short 5-year timescale of these studies.
[7] The HadCM3LC model is run from 1860-2100 under transient IS92a emission scenario, and changes are calculated as the difference between the 1970-2000 average and the 2070-2100 average. The mean atmospheric CO_2 concentration was about 346 ppm from 1970-2000, and scenario IS92a reaches about 700 ppm by 2100.

Appendix B.
DESCRIPTION OF MODELS USED

Modeling Center	Earth System Model Name	Land Model Name	Land Model Abbreviation	Dynamic Vegetation
Beijing Climate Center (BCC)	bcc-csm1-1 (Wu et al. 2014)	Beijing Climate Center Atmosphere – Vegetation Interaction Model Version 1.0	BCC-AVIM1	No
Canadian Centre for Climate Modelling and Analysis (CCCma)	CanESM2 (Arora et al. 2011)	Canadian Terrestrial Ecosystem Model (Arora et al. 2009; Arora and Boer 2010)	CLASS-CTEM	No
National Center for Atmospheric Research (NCAR)	CESM1-BGC (Hurrell et al. 2013; Lindsay et al. 2014)	Community Land Model Version 4 (Oleson et al. 2010; Lawrence et al. 2011)	CLM4	No
NOAA Geophysical Fluid Dynamics Laboratory (GFDL)	GFDL-ESM2M (Dunne et al. 2012)	GFDL Land Model 3.0 (Dunne et al. 2012)	LM3	Yes
Met Office Hadley Centre (MOHC)	HadGEM2-ES (Collins et al. 2011; Martin et al. 2011)	Top-down Representation of Interactive Foliage and Flora Including Dynamics	TRIFFID	Yes
Institut Pierre Simon Laplace (IPSL)	IPSL-CM5A-LR (Dufresne et al. 2013)	Organizing Carbon and Hydrology in Dynamic Ecosystems	ORCHIDEE	No
Norwegian Climate Centre (NCC)	NorESM1-ME (Bentsen et al. 2013; Iversen et al. 2013; Tjiputra et al. 2013)	Community Land Model Version 4 (Oleson et al. 2010; Lawrence et al. 2011)	CLM4	No
Max Planck Institute for Meteorology (MPI)	MPI-ESM-LR (Giorgetta et al. 2013)	Jena Scheme for Biosphere–Atmosphere Coupling in Hamburg	JSBACH	Yes

TABLE B1. Description of CMIP5 models used in analysis.

Modeling Center	Earth System Model Name	Land Model Name	Land Model Abbreviation	Dynamic Vegetation
Beijing Climate Center (BCC)	BCC-CSM2-MR (Wu et al. 2019)	Beijing Climate Center Atmosphere – Vegetation Interaction Model Version 2.0	BCC-AVIM2	No
Canadian Centre for Climate Modelling and Analysis (CCCma)	CanESM5 (Swart et al. 2019)	Canadian Terrestrial Ecosystem Model (Arora et al. 2009; Arora and Boer 2010)	CLASS-CTEM	No
National Center for Atmospheric Research (NCAR)	CESM2 (Danabasoglu et al.)	Community Land Model Version 5 (Lawrence et al. 2019)	CLM5	No
NOAA Geophysical Fluid Dynamics Laboratory (GFDL)	GFDL-ESM4	GFDL Land Model version 4.1	LM4p1	Yes
Met Office Hadley Centre (MOHC)	UKESM1-0-LL (Sellar et al. 2019)	Joint UK Land Environment Simulator	JULES-ES-1.0	Yes
Institut Pierre Simon Laplace (IPSL)	IPSL-CM6A-LR	Organizing Carbon and Hydrology in Dynamic Ecosystems, branch 2.0	ORCHIDEE, branch 2.0	No
Centre National de Recherches Météorologiques (CNRM)	CNRM-ESM2-1 (Séférian et al. 2019)	Interaction Soil-Biosphere-Atmosphere (Decharme et al. 2019)	ISBA-CTRIP	No
NASA Goddard Institute for Space Studies (NASA-GISS)	GISS-E2-1-G	GISS Land Surface Model	GISS LSM	No
Japan Agency for Marine-Earth Science and Technology (JAMSTEC)	MIROC-ES2L (Hajima et al. Submitted)	Vegetation Integrative SImulator for Trace gases model (Ito and Inatomi 2011; Hajima et al. Submitted)	VISIT-e	No
Max Planck Institute for Meteorology (MPI)	MPI-ESM1.2- LR (Mauritsen et al. 2019)	Jena Scheme for Biosphere–Atmosphere Coupling in Hamburg	JSBACH3.2	Yes
Norwegian Climate Centre (NCC)	NorESM2-LM	Community Land Model Version 5 (Lawrence et al. 2019)	CLM5	No
Commonwealth Scientific and Industrial Research Organization (CSIRO)	ACCESSESM1.5	Community Atmosphere Biosphere Land Exchange	CABLE2.4 with CASA-CNP	No

TABLE B2. Description of CMIP6 models used in analysis.

Appendix C.
NONLINEARITIES BETWEEN THE PHYSIOLOGICAL AND RADIATIVE EFFECTS OF CO_2

Nonlinearities between the physiological and radiative effects of increasing CO_2 can result in differences in physiologically-driven climate changes between FULL-RAD (which includes any nonlinear interactions) and PHYS-PI (which does not include nonlinear interactions). We refer to the effect of these nonlinear interactions as the interaction term, which we calculate as the difference between FULL-RAD and PHYS-PI. On global scales, there is poor model agreement on the sign of the interaction term. At $2xCO_2$ and $4xCO_2$, some models show more physiologically-driven warming in PHYS-PI than FULL-RAD and some models show the opposite, resulting in a negligible interaction term in the multi-model mean globally and over non-glaciated land (Figures C1 and C2). However, in some regions there is better model coherence on the sign of the interaction term. For example, at $2xCO_2$, most models show physiologically-driven warming in the Southern Ocean, especially the Weddell Sea, in PHYS-PI but not in FULL-RAD (Figure E1). At 4xCO2, most models show more physiologically-driven warming in PHYS-PI than FULL-RAD in the tropics and eastern United States (Figure E2), though the interaction term in these regions is much smaller than FULL-RAD or PHYS-PI.

There are several mechanisms that could drive nonlinearities between the physiological and radiative effects of increasing CO_2. The magnitude of physiologically-driven changes in evapotranspiration depends on both reference system leaf area and stomatal conductance (Equation 1), so radiatively-driven changes in these quantities can result in nonlinearities in evapotranspiration changes

and therefore temperature. For example, radiatively-driven warming generally increases leaf area in high-latitudes (Keenan and Riley 2018), while some ESMs suggest warming may decrease vegetation productivity and leaf area in the tropics (Mahowald et al. 2016). Differences in sea ice extent between RAD and PI could also lead to nonlinearities in the Earth System response to physiologically-driven perturbations to the land surface, since sea ice feedbacks are nonlinear with temperature (Goosse et al. 2018) and multiple studies have found that vegetation changes can drive changes in sea ice extent (Laguë and Swann 2016; Kim et al. 2020; Park et al. 2020). Alternatively, internal variability of the Earth System could result in differences between FULL-RAD and PHYS-PI that do not represent a robust, physically meaningful interaction term.

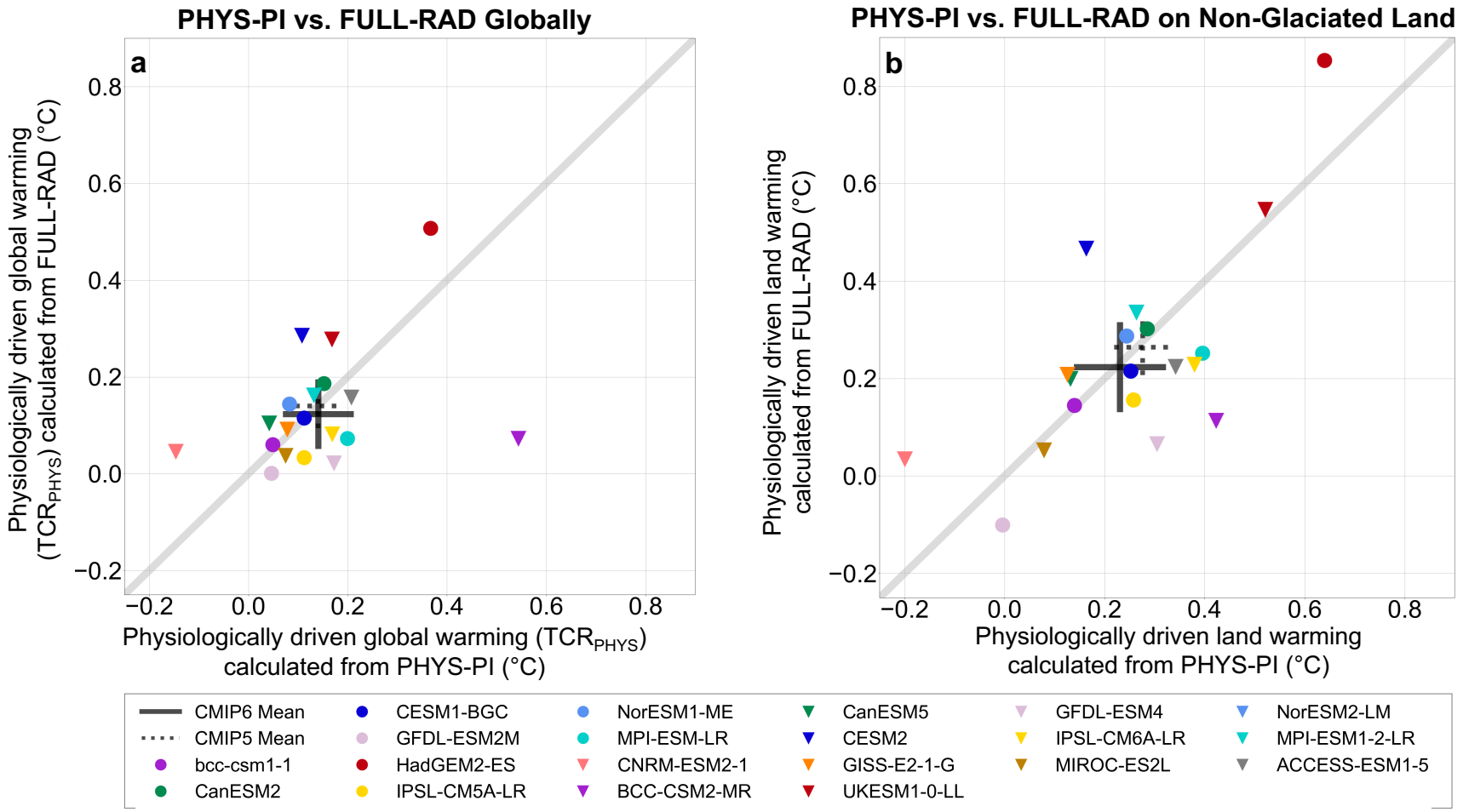

FIGURE C1. Comparison of the physiological contribution to warming at 2xCO_2 as calculated by PHYS-PI vs. as calculated by FULL-RAD in (a) the global mean and (b) over non-glaciated land. The gray 1:1 line is where we would expect all models to be if there were no nonlinear interactions between the radiative and physiological effects of increasing CO_2. Marker types indicate CMIP phase (CMIP5: circles; CMIP6: triangles) and colors indicate modeling center. Crosses mark multi-model means (black) for CMIP6 (solid) and CMIP5 (dashed), and the width of each cross corresponds to two times the ensemble mean standard deviation in global mean near-surface temperatures from the preindustrial control (a) globally and (b) over non-glaciated land. NorESM2-LM is not included in this figure because PHYS model output was not available for NorESM2-LM.

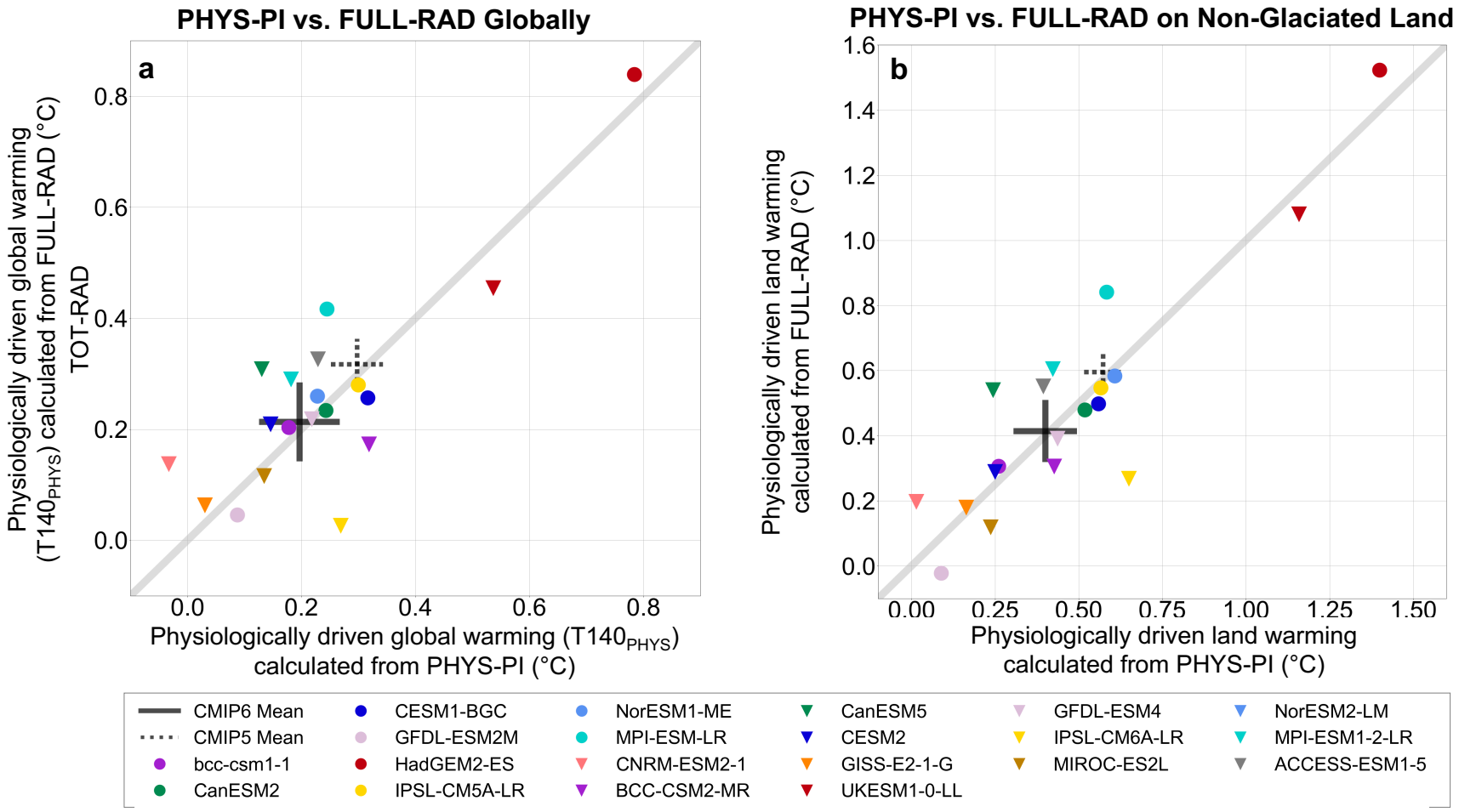

FIGURE C2. Comparison of the physiological contribution to warming at 4xCO_2 as calculated by PHYS-PI vs. as calculated by FULL-RAD in (a) the global mean and (b) over non-glaciated land. The gray 1:1 line is where we would expect all models to be if there were no nonlinear interactions between the radiative and physiological effects of increasing CO_2. Marker types indicate CMIP phase (CMIP5: circles; CMIP6: triangles) and colors indicate modeling center. Crosses mark multi-model means (black) for CMIP6 (solid) and CMIP5 (dashed), and the width of each cross corresponds to two times the ensemble mean standard deviation in global mean near-surface temperatures from the preindustrial control (a) globally and (b) over non-glaciated land. NorESM2-LM is not included in this figure because PHYS model output was not available for NorESM2-LM.

Appendix D.
DERIVATION OF EQUATION 1

We derive an equation to partition the total physiologically-driven change in evapotranspiration (ET) into its component physiological drivers by first expressing ET as a function of transpiration per leaf area, leaf area, and evaporation, as shown in Equation D1:

$$ET = T + E = \left(\frac{T}{L}\right) L + E \qquad \text{Equation D1}$$

where ET = evapotranspiration (mm/day), T = transpiration (mm/day), E = evaporation (mm/day), and L = leaf area index (unitless). We then express the physiologically-driven change in total ET (ΔET) as the difference between ET in the WITH PHYS and REF experiments ($ET_{WITH\ PHYS}$ and ET_{REF}, respectively) and express these in terms of T/L, L, and E as in Equation D1. WITH PHYS and REF correspond to FULL and RAD when calculating physiologically-driven changes from FULL-RAD, and WITH PHYS and REF correspond to PHYS and PI when calculating physiologically-driven changes from PHYS-PI.

$$\Delta ET = ET_{WITH\ PHYS} - ET_{REF} = \left(\left(\frac{T}{L}\right) L + E\right)_{WITH\ PHYS} - \left(\left(\frac{T}{L}\right) L + E\right)_{REF} \qquad \text{Equation D2}$$

We then rearrange the terms in Equation D2 as shown in Equations D3 - D5.

$$\Delta ET = \left[\left(\frac{T}{L}\right)_{WITH\ PHYS} L_{WITH\ PHYS}\right] - \left[\left(\frac{T}{L}\right)_{REF} L_{REF}\right] + [E_{WITH\ PHYS} - E_{REF}] \qquad \text{Equation D3}$$

$$\Delta ET = \left(\left(\frac{T}{L}\right)_{REF} + \Delta\frac{T}{L}\right)(L_{REF} + \Delta L) - \left(\frac{T}{L}\right)_{REF} L_{REF} + \Delta E \qquad \text{Equation D4}$$

$$\Delta ET = \left(\left(\frac{T}{L}\right)_{REF} + \Delta\frac{T}{L}\right) L_{REF} + \left(\left(\frac{T}{L}\right)_{REF} + \Delta\frac{T}{L}\right)\Delta L - \left(\frac{T}{L}\right)_{REF} L_{REF} \ + \Delta E \qquad \text{Equation D5}$$

This results in Equation D6 (which corresponds to Equation 1 in the main text), which expresses the total physiologically-driven change in ET in terms of physiologically-driven changes in L, T/L, and E:

$$\Delta ET = \left(\frac{T}{L}\right)_{REF} \Delta L + L_{REF}\, \Delta\left(\frac{T}{L}\right) + \Delta\frac{T}{L}\Delta L \ + \Delta E \qquad \text{Equation D6}$$

where the four terms on the right-hand side of Equation D6 correspond to the physiologically-driven change in ET due to (1) changes in LAI, (2) changes in stomatal conductance, as approximated by transpiration per LAI, (3) the interaction between changes in LAI and changes in stomatal conductance, and (4) changes in evaporation.

Appendix E.
MODEL AGREEMENT

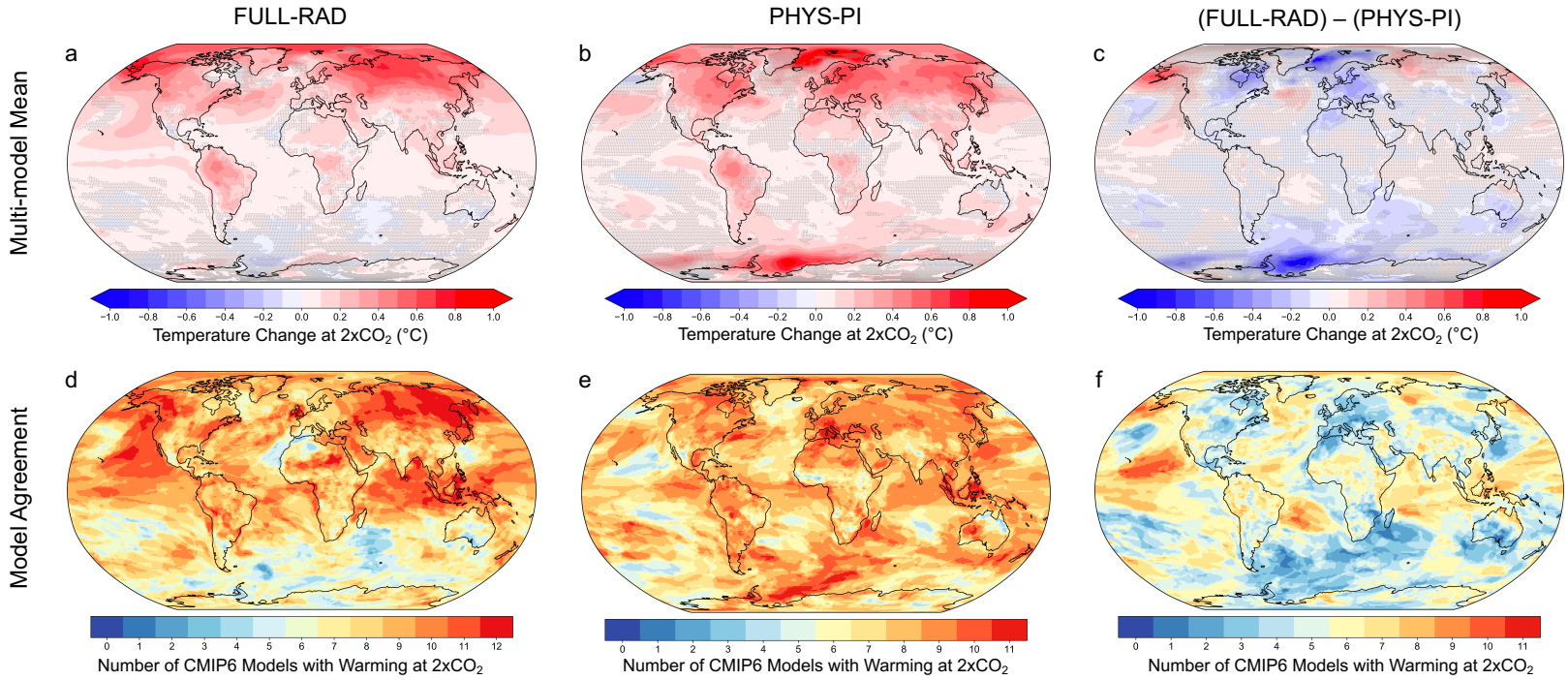

FIGURE E1. Spatial pattern of warming and model agreement at $2xCO_2$. The top row depicts the multi-model mean of the magnitude of physiologically-driven near-surface air temperature change at $2xCO_2$ (a) as calculated by FULL-RAD, (b) as calculated by PHYS-PI, and (c) the interaction term between the radiative and physiological effects of CO_2 as calculated by (FULL-RAD) – (PHYS-PI). Stippling indicates regions where less than 8 models agree on the sign of change, out of 12 CMIP6 models for (a) and out of 11 CMIP6 models for (b) and (c) The bottom row depicts model agreement on the sign of near-surface air temperature change for (a) FULL-RAD, (e) PHYS-PI, and (f) the interaction term as calculated by (FULL-RAD) – (PHYS-PI). Darker reds in (d) and (e) indicate regions where most models agree that the physiological effect results in warming, and darker blues indicate regions where most models agree that the physiological effect results in cooling. In (f), darker reds indicate regions where models agree that TOT-RAD is larger than PHYS-PI, darker blues indicate regions where most models agree that PHYS-PI is larger than TOT-RAD, and yellows indicate poor model agreement.

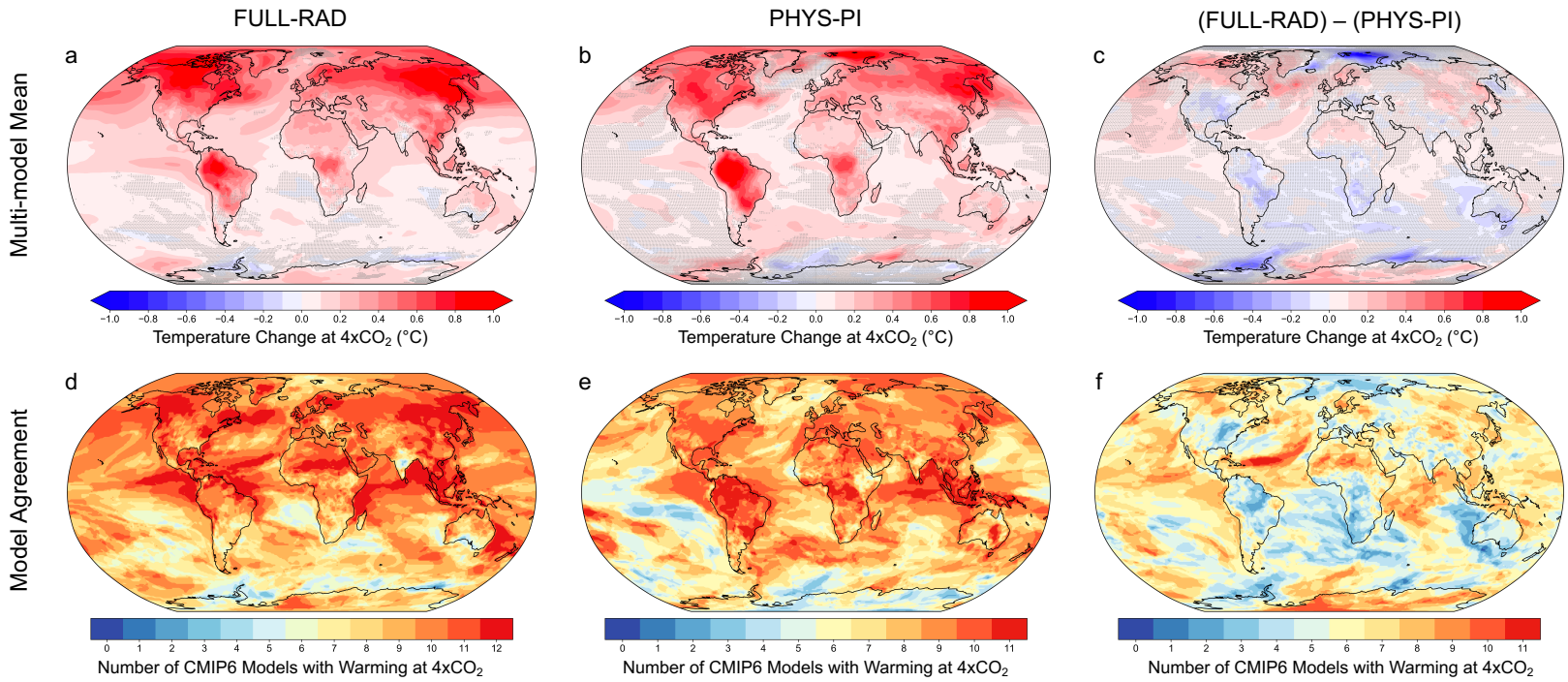

FIGURE E2. Spatial pattern of warming and model agreement, as in Figure E1, at $4xCO_2$.

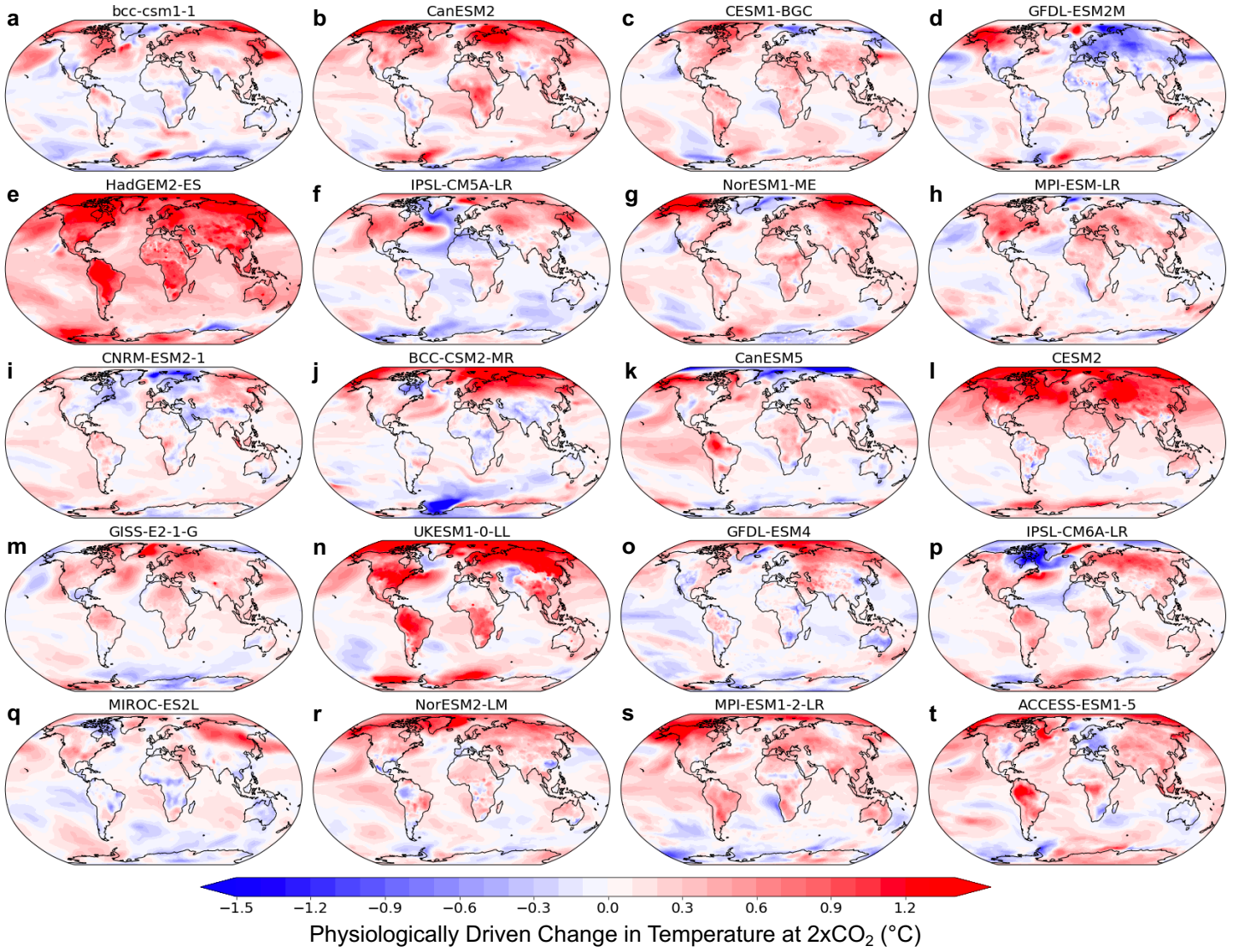

FIGURE E3. Spatial pattern of temperature change at 2xCO_2 (years 61-80) for CMIP5 (a-h) and CMIP6 (i-t) ESMs, as calculated by FULL-RAD.

Appendix F.
INTERNAL VARIABILITY AND SIGNIFICANCE TESTING

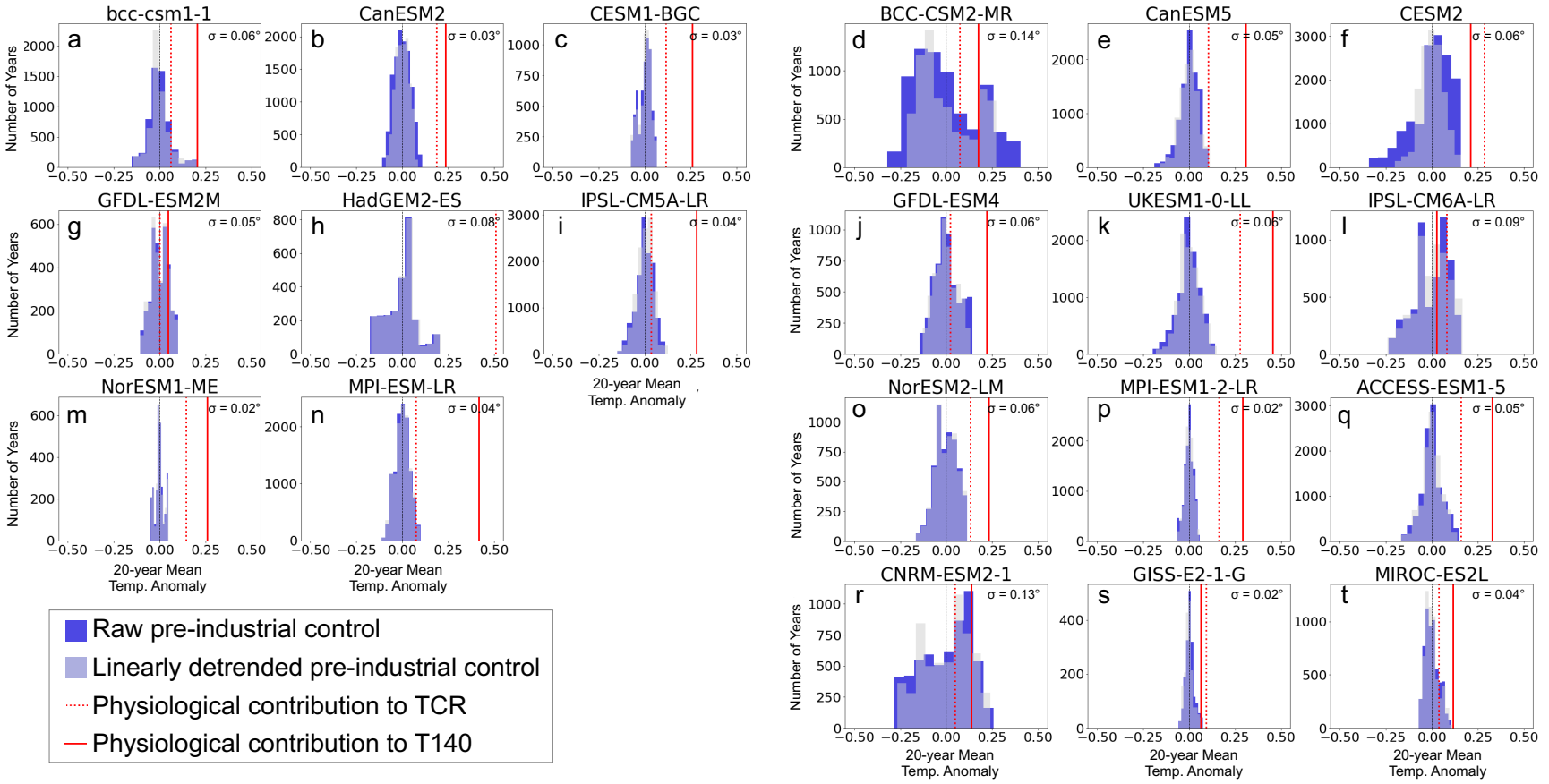

FIGURE F1. Histograms showing the distribution of the 20-year running mean global temperature anomalies in the pre-industrial control experiment (PI). Dark blue indicates the anomalies relative to the global temperature as averaged over the entire PI time series, and light blue-grey indicates the anomalies after linear detrending of the entire PI time series. Dotted and solid red lines show the physiological contribution to the TCR and T140, respectively. In order to maintain consistent x-axes across subpanels, T140 for HadGEM2-ES (0.84°C) is not shown in panel h. Standard deviations of the linearly detrended 20-year mean temperature anomalies are reported for each model in the upper right corner of each panel. The first three columns (a, b, c, g, h, i, m, n) are CMIP5 models, and the third through sixth columns (d, e, f, j, k, l, o, p, q, r, s, t) are CMIP6 models.

Model Name	Global (All Land and Ocean)			Non-glaciated Land		
	Pre-industrial SD (°C)	2xCO_2 p-value	4xCO_2 p-value	Pre-industrial SD (°C)	2xCO_2 p-value	4xCO_2 p-value
bcc-csm1-1	0.059	0.15	*<0.01**	0.047	*<0.01**	*<0.01**
CanESM2	0.035	*<0.01**	*<0.01**	0.046	*<0.01**	*<0.01**
CESM1-BGC	0.033	*<0.01**	*<0.01**	0.045	*<0.01**	*<0.01**
GFDL-ESM2M	0.047	0.49	-	0.064	0.94	-
HadGEM2-ES	0.085	*<0.01**	*<0.01**	0.113	*<0.01**	*<0.01**
IPSL-CM5A-LR	0.044	0.22	*<0.01**	0.061	*<0.01**	*<0.01**
MPI-ESM-LR	0.040	*0.03**	*<0.01**	0.061	*<0.01**	*<0.01**
NorESM1-ME	0.024	*<0.01**	*<0.01**	0.016	*<0.01**	*<0.01**
Number of CMIP5 Models with Significant Warming		**5 of 8**	**7 of 7**		**7 of 8**	**7 of 7**
ACCESS-ESM1-5	0.054	*<0.01**	*<0.01**	0.075	*<0.01**	*<0.01*
BCC-CSM2-MR	0.142	0.30	0.11	0.121	0.17	*<0.01**
CanESM5	0.048	*0.01**	*<0.01**	0.065	*<0.01**	*<0.01**
CESM2	0.062	*<0.01**	*<0.01**	0.090	*<0.01**	*<0.01**
CNRM-ESM2-1	0.130	0.36	0.15	0.190	0.43	0.15
GFDL-ESM4	0.060	0.36	*<0.01**	0.046	0.08	*<0.01**
GISS-E2-1-G	0.023	*<0.01**	*<0.01**	0.039	*<0.01**	*<0.01**
IPSL-CM6A-LR	0.092	0.19	0.39	0.135	0.05*	*0.02**
MIROC-ES2L	0.037	0.15	*<0.01**	0.055	0.17	*0.02**
MPI-ESM1-2-LR	0.023	*<0.01**	*<0.01**	0.035	*<0.01**	*<0.01**
NorESM2-LM	0.059	*0.01**	*<0.01**	0.101	*0.02**	*<0.01**
UKESM1-0-LL	0.056	*<0.01**	*<0.01**	0.077	*<0.01**	*<0.01**
Number of CMIP6 Models with Significant Warming		**7 of 12**	**9 of 12**		**8 of 12**	**11 of 12**

TABLE F1. Statistical significance of physiologically-driven warming (as calculated by FULL-RAD) for CMIP5 and CMIP6 models. Significance is tested against the distribution of 20-year running mean detrended temperatures in the PI control experiments (i.e. the distribution in Figure F1). p-values which indicate statistical significance at 95% confidence are indicated with an asterisk and emphasized in italics. Values are not reported for GFDL-ESM2M at 4xCO_2 because this model stopped increasing CO_2 concentration after reaching 2xCO_2.

VITA

Claire Zarakas is an Atmospheric Sciences graduate student and Department of Energy Computational Science Graduate Fellow in the Ecoclimate Lab at the University of Washington. Prior to joining the Ecoclimate Lab, she worked at a public sector consulting firm where she conducted research to inform climate mitigation and adaptation policies. She graduated summa cum laude from Princeton University in 2016, where she was a Geosciences major and focused on climate science, ecology, and biogeochemistry in her coursework and research.